9. SITE 1070[1]

Shipboard Scientific Party[2]

HOLE 1070A

Position: 40°47.779′N, 12° 43.430′W

Start hole: 1900 hr, 31 May 1997

End hole: 0415 hr, 7 June 1997

Time on hole: 153.25 hr (6.4 days)

Seafloor (drill pipe measurement from rig floor, mbrf): 5333.0

Total depth (drill pipe measurement from rig floor, mbrf): 6051.8

Distance between rig floor and sea level (m): 11.2

Water depth (drill pipe measurement from sea level, m): 5321.8

Penetration (mbsf): 718.8

Coring totals:

Type: RCB; Number: 14; Cored: 119.8 m; Recovered: 51.77 m; Average recovery: 43.2%

Sedimentary sequence:

Subunit IIC: (599.0–619.0 mbsf): claystone and silty claystone (early Oligocene to late Eocene?)
Unit III: (619.0–657.97 mbsf): claystone and silty claystone (barren)
Unit IV: (657.97–658.37 mbsf): nannofossil chalk, calcareous chalk, and breccia (late Aptian)

Basement:

Unit 1: (658.37–676.2 mbsf): poorly sorted breccia with serpentinite clasts in a calcite matrix
Subunit 2A:(676.2–679.74 mbsf): very coarse-grained (pegmatitic) gabbro
Subunit 2B: (679.74–718.8 mbsf): serpentinized peridotite

Principal results: Site 1070 lies over an elongated basement ridge about 15 km east of the crest of the J magnetic anomaly and 20 km west of the peridotite ridge. Both ridges lie parallel to the continental margin. The main objective at this site was to sample basement at the western end of the OCT where oceanic crust is inferred by geophysical data, to characterize the petrological nature and emplacement mode of the early formed oceanic crust.

The principal result from Hole 1070A is that the basement consists of (from top to bottom) tectonosedimentary breccias, a body of pegmatitic gabbro, and serpentinized peridotite intruded by gabbroic veinlets that have been highly altered to low-grade or very low-grade assemblages. Contrary to expectations, no rocks from the upper oceanic crust (basaltic lavas or sheeted dikes) were encountered. Protolith assemblages suggest that the peridotites were lherzolites, harzburgites, and dunites.

A 59.34-m-thick, lower Oligocene to late Aptian sedimentary succession was cored. It is divided into three lithostratigraphic units. The site was located in deeper water, farther from turbidite sources, and over a higher basement high than other sites drilled in this area. Consequently, the cores recovered more hemipelagic sediments and less carbonate than in equivalent sections at the other sites, and calcareous fossils were recovered only near the top (lithostratigraphic Subunit IIC, Paleogene) and bottom (lithostratigraphic Unit IV, Lower Cretaceous) portions of the cored sequence. Coring commenced in the >20-m-thick Subunit IIC, which consists of upward-darkening sequences of calcareous to nannofossil claystone overlain by claystone that were deposited as calcareous turbidites and noncarbonate hemipelagites, probably near or below the carbonate compensation depth (CCD). Unit III consists of barren brown claystones that are 39 m thick. They are interpreted as the product of slow accumulation of clay in an oxygenated environment on the abyssal plain below the CCD. Manganese micronodules in the claystones also indicate a low rate of deposition. Thin beds of sand near the base may have been deposited as turbidites (one is normally graded) and may be distal equivalents of the high-density turbidites present in Subunit IIIB at Site 897.

The boundary between Units III and IV is taken at the change from brown claystone to nannofossil claystone at 1070A-7R-2, 17 cm. In Unit IV, matrix-supported sedimentary breccias are interbedded with nannofossil chalk. The breccias are 3–4 cm thick and normally graded. They were probably deposited as small debris flows or turbidites that transported locally derived material relatively short distances. The chalk is pelagic in origin and was deposited above the CCD. The petrographic features of the calcareous chalks interbedded with the breccias strongly suggest that their constituent calcite grains are largely detrital. The likely source of the calcite clasts is the underlying calcitized basement material. Nannofossils present in the chalks indicate an Aptian age. The recovery of agglutinated foraminiferal assemblages characteristic of deep-water habitats and the paucity of sediment input of grain size larger than 63 µm suggest that the environment of deposition was probably at bathyal depths during the Aptian, after which it remained below the CCD.

The basement is divided into two units reflecting the dominant petrological features of each. Unit 1 consists of matrix-supported breccias of serpentinized peridotite and rare, weakly deformed, coarse-grained gabbro. The matrix consists of several generations of calcite, including spherical aggregates (botryoidal calcite). Serpentinization preceded calcite precipitation (serpentinite mesh structures are cut by calcite veins). Abundant “jigsaw” clasts and the transition downward into an incohesive fault gouge suggest a predominantly tectonic origin for these breccias.

The occurrence of tectonosedimentary breccias and gouge on top of serpentinized peridotite, observed during Legs 149 (Site 897) and 173 (Sites 1068 and 1070), is related to a late stage of emplacement of the mantle rocks on the seafloor. However, to what extent the breccias are formed by sedimentary processes and/or result from brecciation along fault planes is not yet clear.

The contact between Units 1 and 2 consists of a short interval of highly sheared serpentinite over pegmatitic gabbro. Unit 2 is divided into two subunits: the 3.5-m-thick Subunit 2A made of pegmatitic gabbro and the 39-m-thick Subunit 2B made of serpentinized peridotite intruded by a few 1- to 4-cm-thick altered gabbroic dikes. The gabbro of Subunit 2A shows a clear intrusive contact with the underlying serpentinized peridotites. It is locally weakly foliated. The peridotite, generally strongly serpentinized, displays variable amounts of pyroxene, from pyroxenitic layers to a more dunitic layer. A high-temperature foliation is only locally marked by the alignment of spinels and pseudomorphs after pyroxenes; it is generally weak and shallowly to moderately inclined (between 9° and 45°). These observations suggest that the peridotites were only weakly deformed at high temperature. The presence of gabbroic veins demonstrates that a later stage of brittle deformation might have occurred in the mantle rocks during the emplacement of the intrusives.

Results from the pass-through cryogenic magnetometer measurements and discrete sample demagnetization experiments indicate that two

[1]Whitmarsh, R.B., Beslier, M.-O., Wallace, P.J., et al., 1998. *Proc. ODP, Init. Repts.*, 173: College Station, TX (Ocean Drilling Program).
[2]Shipboard Scientific Party is given in the list preceding the Table of Contents.

or three magnetic polarity reversals may be recorded in the cores. Unfortunately, biostratigraphic ages are not available for these cores, except to suggest that these reversals fall in a period between lower Oligocene and late Cretaceous. Shore-based biostratigraphic and isotopic studies, as well as additional paleomagnetic samples from these intervals, are needed to date and further characterize these reversals. The most interesting result generated from the preliminary shipboard study is the identification of what appears to be a reversely magnetized zone in the serpentinized peridotites (Subunit 2B). The inclinations in Cores 8R to 13R are stable and show a consistent polarity pattern in a zone about 25 m thick. Within this zone, the magnetic inclinations of the samples are predominantly negative (reversed polarity). In contrast, the magnetic inclinations of samples both above and below this zone are almost all positive (normal polarity). This same pattern, also found in the serpentinized peridotites recovered from nearby Leg 149, Sites 897 and 899, suggests that the Iberian peridotites preserved a Cretaceous magnetic record. Further analyses of this magnetic polarity zone, integrated with shore-based geochronologic and isotopic studies, may provide a unique opportunity for dating the tectonic processes that accompanied continental breakup and opening of the North Atlantic.

The poorly consolidated clays, which dominate the sedimentary section, have the lowest bulk densities (1.8 to 2.0 g/cm^3) and highest porosities (44% to 54%) measured during Leg 173. The velocities of all sediment samples from above 635 mbsf are less than 2000 m/s, and only two sediment samples in the lower part of Unit III have higher velocities of ~2200 m/s. The magnetic susceptibility values in Subunit IIC are less than 100×10^{-5} SI units and those in Unit III are between 100×10^{-5} and 400×10^{-5} SI units. There is a 1000×10^{-5} SI units peak of magnetic susceptibility around 649 mbsf in Unit III. Gamma-ray activity is generally between 70 and 80 counts per second (cps) in Subunit IIC and has a peak of over 110 cps at 612 mbsf. Gamma-ray activity decreases to between 60 and 70 cps in Unit III and a peak of over 80 cps lies at 649 mbsf. All basement samples but one have velocities over 4000 m/s and the maximum value is greater than 7000 m/s. Breccia and serpentinite samples from acoustic basement have bulk densities from 2.3 to 2.5 g/cm^3 and porosities from 7% to 17%. Basement rocks have a much higher magnetic susceptibility from a few hundreds of SI units to over 4000×10^{-5} SI units. Gamma-ray values of basement rocks are less than half of those of sediments.

BACKGROUND AND OBJECTIVES

This site (Fig. 1) lies 20 km west of a peridotite ridge (PR; Shipboard Scientific Party, 1994a). The landward edge of oceanic crust off western Iberia is often considered to coincide with this ridge, which is about 15 km wide and runs parallel to the margin for almost 400 km from Galicia Bank to the southernmost Iberia Abyssal Plain (Beslier et al., 1993; Boillot et al., 1980, 1988; Sawyer, Whitmarsh, Klaus, et al., 1994; Sibuet et al., 1995; Whitmarsh and Miles, 1995; Whitmarsh et al., 1996a). However, basement outcrops of peridotite have been cored or inferred at other locations within the southern Iberia Abyssal Plain ocean/continent transition (OCT; Shipboard Scientific Party, 1994b; "Site 898" section in Whitmarsh et al. [1996a]; "Site 1068" chapter, this volume), and the significance and uniqueness of the PR, in relation to it marking the landward edge of oceanic crust, have been questioned (Whitmarsh and Sawyer, 1996).

Magnetic observations also reveal the significance of the location of Site 1070. The well-known, very high-amplitude J magnetic anomaly lies 15 km west of the site (Fig. 1). This anomaly has been recognized in the North Atlantic between the latitudes of Galicia Bank and northwest Africa (Rabinowitz et al., 1979; Masson and Miles, 1984) and off the conjugate margins (Rabinowitz et al., 1978; Tucholke and Ludwig, 1982); it has an approximate age of M0–M2 on the magnetic reversal time scale (i.e., it approximates an isochron). This age has been tentatively confirmed in the southern Iberia Abyssal Plain by seafloor-spreading models of east-west magnetic anomaly profiles that were obtained both at the sea surface and near the sea bed (Whitmarsh and Miles, 1994, 1995; Whitmarsh et al., 1990; Whitmarsh et al., 1996a). However, the correlation of computed and observed anomalies is not always straightforward and, to fit their observations, Whitmarsh et al. (1996a) had to propose spreading rates of 10 and 14 mm/yr along two separate deep-towed, and therefore relatively high-resolution, east-west magnetometer profiles on either side of the site and only about 25 km apart (Fig. 2). In both models, however, the site is predicted to lie toward the oceanward edge of the anomaly M3, reversely magnetized crustal block. Confirmation, by isotope geochronology or by biostratigraphy, of the age of the crust at this site would constrain the pre-J seafloor-spreading rate, and it would be an important consideration for models of early post-breakup magmatic processes.

The site also falls within a region where the seismic crustal thickness is unusually thin. Two independent seismic refraction experiments in the southern Iberia Abyssal Plain have detected oceanic crustal velocity structures, within a few tens of kilometers to the west of the PR that are significantly thinner than the normal 7.0-km-thick Atlantic oceanic crust (White et al., 1992). Whitmarsh et al. (1990) observed an oceanic crust that was only about 5.5 km thick on a north-south line just west of the site (Fig. 3: Disco-161). Dean et al. (1996) report a much more detailed seismic refraction profile, located about 40 km south of the site (IAM-9 in Fig. 2), that shows oceanic crust thickening westward from 5 to over 7 km within 90 km of the PR. A similar, but less well constrained, crustal thickening has also been seismically observed within 40 km of the PR off Galicia Bank (Whitmarsh et al., 1996b). Such thin crust may be widespread along the west Iberia margin (Whitmarsh et al., 1993). The initial, anomalously thin oceanic crust has been explained by a reduced melt supply immediately following the final continental breakup (Bown and White, 1995; Whitmarsh et al., 1993); a reduced melt supply has also been proposed to explain observations of thin ocean crust at a slow-spreading ridge (Cannat, 1993). The oceanward thickening is caused by the gradual attainment of "steady-state" seafloor spreading as the cooling effect on ascending melt of the two conjugate continental lithospheric plates diminishes. Limited asthenospheric melting in this situation is expected to lead to a relatively magnesium-poor melt, which should be reflected in the geochemistry of the overlying oceanic crust and the erupted basaltic lavas (White and McKenzie, 1989; White et al., 1992).

Occurrences of rocks associated with early stages of oceanic spreading are known along the west Iberia margin. A massif formed of a laccolith-like body of gabbro, and some rare dikes and pillows of tholeiitic basalts intrusive in mantle peridotite, has been sampled recently by submersible diving at the southern end of the margin on the Gorringe Bank (Girardeau et al., in press). Basalts have been collected from twelve dive sites on the west and northwest flank of Galicia Bank, in association with peridotite and gabbro exposed on the escarpments of normal faults (Boillot et al., 1988, 1995). They were erupted immediately before the onset of seafloor spreading. Dating by $^{40}Ar/^{39}Ar$ of two dive samples indicate an age of formation of about 100 ± 5 Ma (Malod et al., 1993) when the rift was bounded by continental, or at least transitional, material (Boillot et al., 1995; Kornprobst et al., 1988; Malod et al., 1993). These basalts appear to have compositions close to the limit between the tholeiitic and alkali basalt fields. The only other known basalts were dredged by Matthews (1962) from Swallow Bank (41°21′N, 14°28′W), but these had been almost entirely altered by prolonged exposure at the seafloor.

The major objectives of this site were to establish the presence of oceanic crust, to determine the age and geochemistry of this crust,

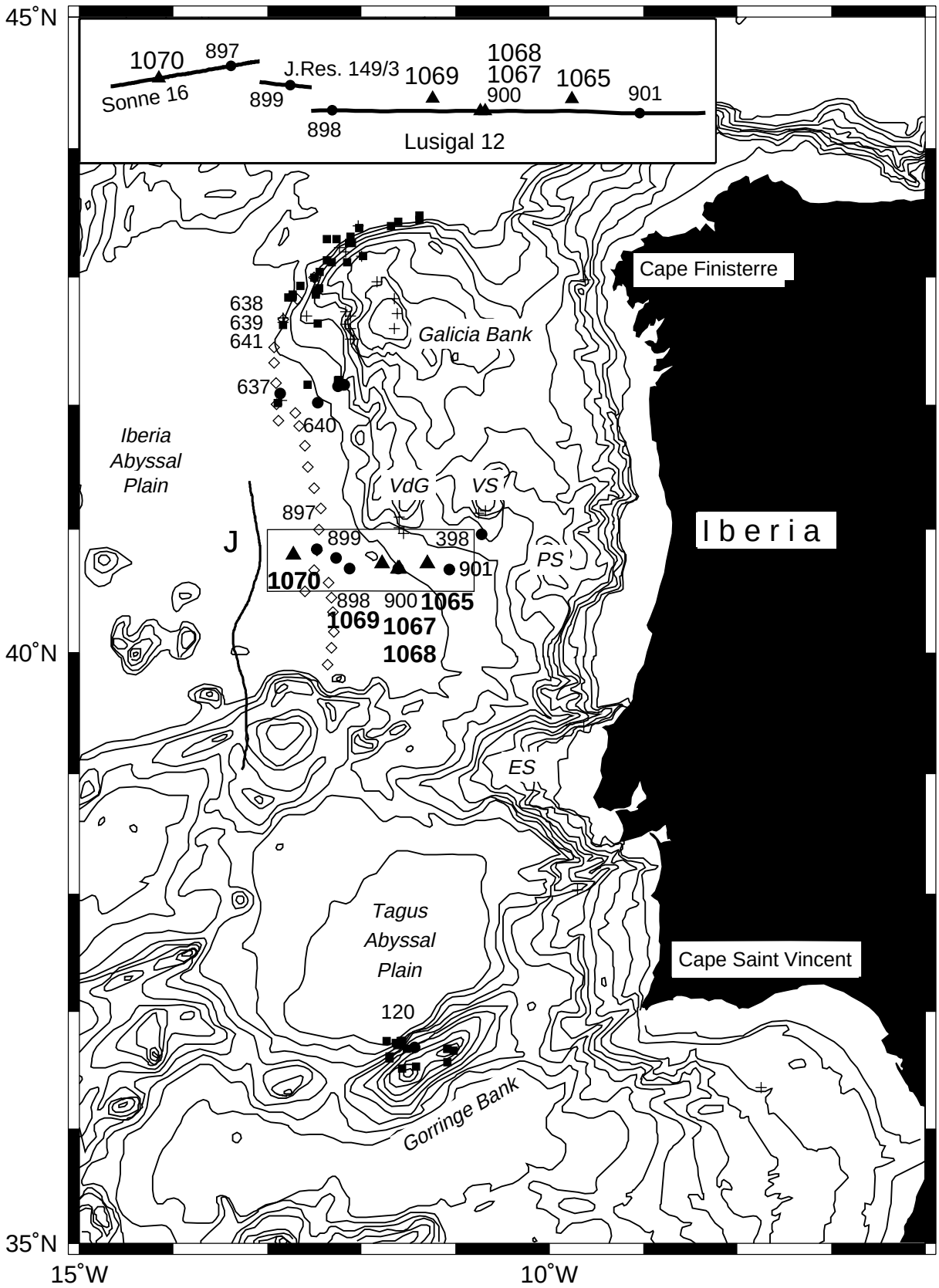

Figure 1. Contoured bathymetric chart of the west Iberia margin. Contours at 500-m intervals. Leg 173 sites are shown by triangles with bold numbers; site drilled on earlier legs are shown by solid circles. J = J magnetic anomaly. PS, VS, and VdG = Porto, Vigo, and Vasco da Gama Seamounts, respectively. ES = Estremadura Spur. Solid squares and crosses denote rock samples obtained by submersible and dredge, respectively. Diamonds denote the location of the crest of the peridotite ridge (PR) of Beslier et al. (1993). The inset is a composite of seismic tracks showing the relative locations of Leg 173 and other drill sites.

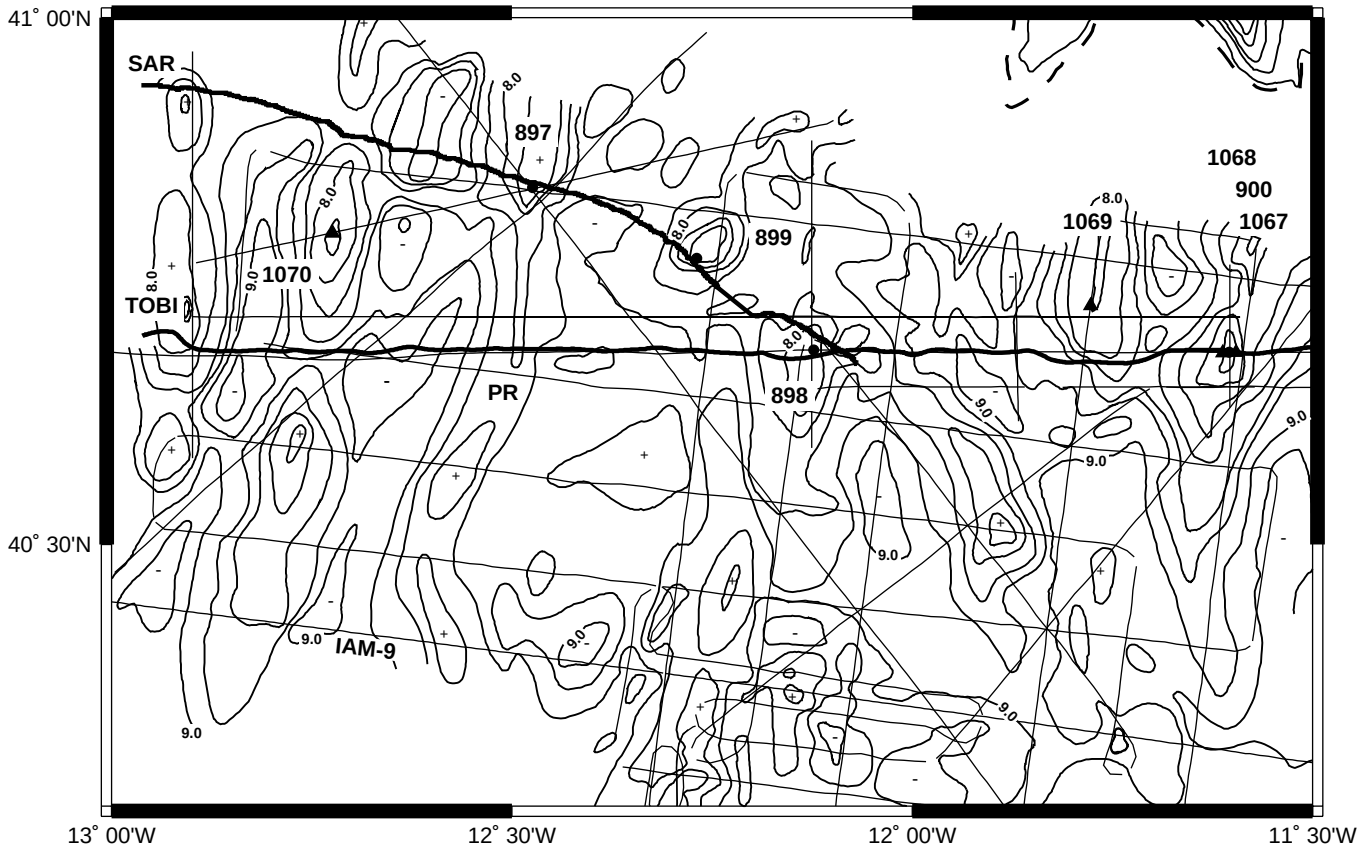

Figure 2. Contour chart of two-way traveltime (TWT) to basement (contour interval 0.25 s TWT, ~250 m; contouring based on work by C.M. Krawczyk, L.M. Pinheiro, S.M. Russell, and R.B. Whitmarsh) combined with bathymetry of the relief bordering the Iberia Abyssal Plain (contour interval 250 m; courtesy J-C. Sibuet). Dashed line denotes edge of abyssal plain. Bold lines are tracks of the TOBI and SAR deep-towed magnetometers (see text). Leg 149 and Leg 173 sites are shown by solid circles and solid triangles, respectively. Fine lines are tracks of seismic lines used to contour basement. Selected basement highs and lows are indicated by + and –, respectively. PR = peridotite ridge.

and to provide information that would constrain models of the ocean-continent transition and of the onset and attainment of steady-state seafloor spreading.

Site 1070 is situated on the crest of a north-northeast–trending basement ridge some 20 km west of the PR drilled at Site 897 during Leg 149 (Shipboard Scientific Party, 1994a). The basement ridge is the first basement high west of the PR. It lies parallel to the PR, is at least 50 km long and has a maximum relief of the order of 0.8 s TWT (~800 m) in the vicinity of the site (Figs. 2, 4). The site is crossed by a single multichannel seismic reflection profile that indicates the presence of 0.67 s TWT (~650 m) of postrift sediment (Fig. 4).

OPERATIONS

The 44-nm distance from Site 1069 to Site 1070 (proposed site IBERIA-10A) was covered in 4.25 hr at an average speed of 10.4 kt. At 1900 hr on 31 May 1997, a positioning beacon was deployed, thrusters and hydrophones were lowered, and by 1930 hr the vessel was stabilized over the drilling location. A new core bit and mechanical bit release were made up, and the drill string was tripped to the seafloor. At 2045 hr on 31 May, a back-up positioning beacon was deployed. Hole 1070A was spudded with the RCB center bit assembly at 0445 hr on 1 June, at a seafloor depth of 5333.0 mbrf. At 20 mbsf, the driller noted higher than normal pump pressure, which continued sporadically throughout the drilling operations at this site. Intermittent plugging of the bit jets was the suspected cause. After three inspections during drilling, the center bit was recovered at a depth of ~500 mbsf and a core barrel, without a check ball installed, was deployed to see if the rate of advancement would improve. Drilling continued at exactly the same rate (19.2 m/hr) as with the center bit. Drilling proceeded until 2230 hr on 2 June (599.0 mbsf). The wash barrel was then recovered and a core barrel was deployed. Continuous RCB coring continued to a total depth of 718.8 mbsf (Table 1). Crystalline basement, largely made up of serpentinized peridotite, was identified beginning with Core 7R at ~658.4 mbsf. Finally, Cores 13R and 14R achieved a rate of penetration of only 1.1 m/hr, with recovery of 55% and 71%, respectively.

At 0945 hr on 5 June coring operations were ended and a prelogging wiper trip was begun. While pulling the first stand of drill pipe off the bottom, a 20,000-lb overpull was noted. During the remaining pipe trip to 100 mbsf, there were no indications of hole problems. The trip back to bottom was equally uneventful until a hard obstruction was encountered at 673.0 mbsf, or about 46 m off bottom. While picking up a double pipe stand to insert the top drive, the driller noticed an 80,000 lb overpull on the drill string. Once the top drive was in place, the pipe could be rotated and circulated but only could be worked between the depths of 666.0 and 655.0 mbsf. A sepiolite mud pill was circulated but did nothing to improve the situation. The ability to rotate the pipe was lost and then regained on several occasions although high and erratic torque was experienced throughout the exercise. After working the pipe for nearly 3 hr without any mea-

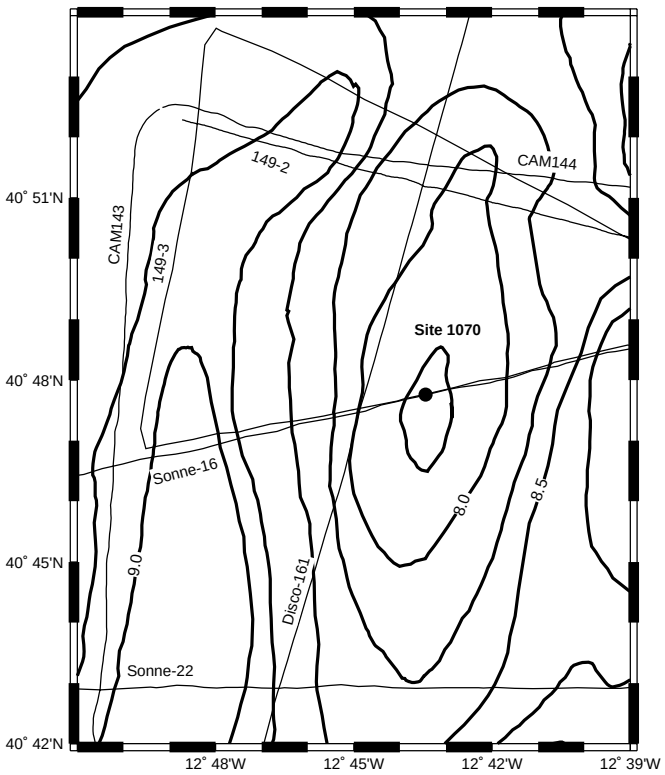

Figure 3. Contours of top of acoustic basement (contour interval 0.25 s TWT, ~250 m) with tracks of seismic reflection profiles in the vicinity of Site 1070. Single channel seismic lines are shown by finer lines. Site 1070 is indicated by a solid circle.

surable success, it was decided that logs in the lower part of the hole were unlikely to be obtained even if the pipe could be freed. The shifting tool was deployed in the hope that the pipe was stuck at the bit and would come free once the bit was released. At 1630 hr the bit was released but the drill string remained stuck. Another 2 hr was spent circulating sepiolite mud and working the pipe with overpulls of up to 150,000 lb over the 630,000 lb hanging weight.

At 1930 hr on 5 June, while continuing to work the stuck drill string, an unusual noise was heard from the drawworks when the low drum clutch was engaged. Further investigation revealed that the hub had spun on the motor shaft of the forward traction motor, separating the drive sprocket from the armature shaft. At the time of the incident no overpull was being applied, and only a static string weight of 630,000 lb was being supported. As a result of the failure, the drawworks was electrically isolated and the input chain was removed from the motor and chain case. No progress had been made up to that point in freeing the drill string and a single drawworks motor did not provide enough hoisting capacity to continue the attempt. Therefore, at 2000 hr on 5 June, drill string severing operations were initiated. The Schlumberger logging line was rigged up and an explosive charge was assembled to sever the stuck drill string above the BHA. The first charge was detonated at 0215 hr on 6 June at a depth of 536.0 mbsf. Approximately 30,000 lb of overpull and 4,000 ft-lb of torque were applied to the drill string at the time. There was no indication that the charge had fired, and the drill string remained stuck. Apparently, the hole had collapsed above the point of detonation. A second charge was detonated at 30 mbsf at 0900 hr on 6 June. This time the drill string came free. The severing tool was retrieved and Schlumberger logging line and sheaves were rigged down.

The drill string trip commenced at 1130 hr on 6 June using the single remaining (aft) drawworks motor. Once repairs were completed, 1.5 hr were taken to reinstall the forward drawworks motor. At 0130 hr on 7 June, with 1982 m of pipe still to be recovered, the trip resumed. The pipe trip was completed at 0415 hr and the rig was secured for transit. In addition to losing a complete BHA, including ten 8-1/4-in drill collars, a tapered drill collar, and 2 stands of 5-1/2-in transition pipe, 16 stands of 5 in drill pipe, and a single severed joint were left in the hole. As a result of the stuck pipe and the resulting severing incident no wireline logging was accomplished.

Weather during the last two days of operations at this site was the worst experienced during the leg. Force 9–10 conditions continued for the last 24–36 hr, eventually moderating to force 8. Sustained winds averaged 33 kt with gusts to 42 kt. Seas and swells averaged 25 ft and 18 ft, respectively. The vessel began the voyage to Halifax, Nova Scotia, at 0415 hr on 7 June, departing the last drill site 7.25 hr behind schedule in force 8 weather conditions. Leg 173 officially ended with the first mooring line ashore in the port of Halifax, Nova Scotia, at 2200 hr on 15 June.

LITHOSTRATIGRAPHY

In Hole 1070A, a 59.37-m-thick, early Oligocene to late Aptian sedimentary succession was cored. The succession consists of claystones, calcareous chalks and nannofossil chalks, and minor clayey sandstones and breccias overlying a 60.4-m succession of tectonic breccias, gabbros, and peridotites. A simplified summary of the lithostratigraphy cored at this site and other Leg 173 and Leg 149 sites is shown in Figure 5.

The lower Oligocene succession cored at this site is assigned to the lower part of Subunit IIC because it is similar to sediments of the same age cored at Sites 897, 899, and 900 (Shipboard Scientific Party, 1994a, 1994b, 1994c), and Sites 1067, 1068, and 1069 (this volume).

The top of Unit III is defined at the base of the deepest upward-darkening sequence typical of Subunit IIC. It consists of brown claystones and variously colored clayey to sandy lithologies that are comparable to the red claystone and conglomerate successions of Unit III drilled at Sites 897 and 899 (Shipboard Scientific Party, 1994a, 1994b).

Between Unit III and the basement breccias, a 37-cm interval of nannofossil chalk with thin basal breccia beds occurs. This interval shows a sharp contact with Unit III. It is designated as Unit IV.

Rotary coring was employed in Hole 1070A, yielding ~53% average recovery for sediments of Unit II and ~43% for those of Unit III. Coring began at 599.0 mbsf (Subunit IIC) and penetrated brecciated basement at 658.37 mbsf, below Unit IV (see "Igneous and Metamorphic Petrology" and "Structural Geology" sections, this chapter). Figure 6 summarizes the core recovery, lithologies, and ages of the lithostratigraphic units recognized in Hole 1070A. The ages, lithologic compositions, colors, facies and depositional environments, boundary depths, and cored intervals of Units II, III, and IV are summarized in Table 2.

Subunit IIC

Interval: 173-1070A-1R-1, 0 cm, through 173-1070A-3R-1, 70 cm
Depth: 599.0–619.0 mbsf
Age: early Oligocene (or barren)

General Description

The sediments in Subunit IIC are firm to hard, and core disturbance is characterized by moderate biscuiting, which obscures most of the internal structures.

Subunit IIC is characterized by sharp-based upward-darkening sequences (2–5 cm thick) that consist of basal calcareous claystone

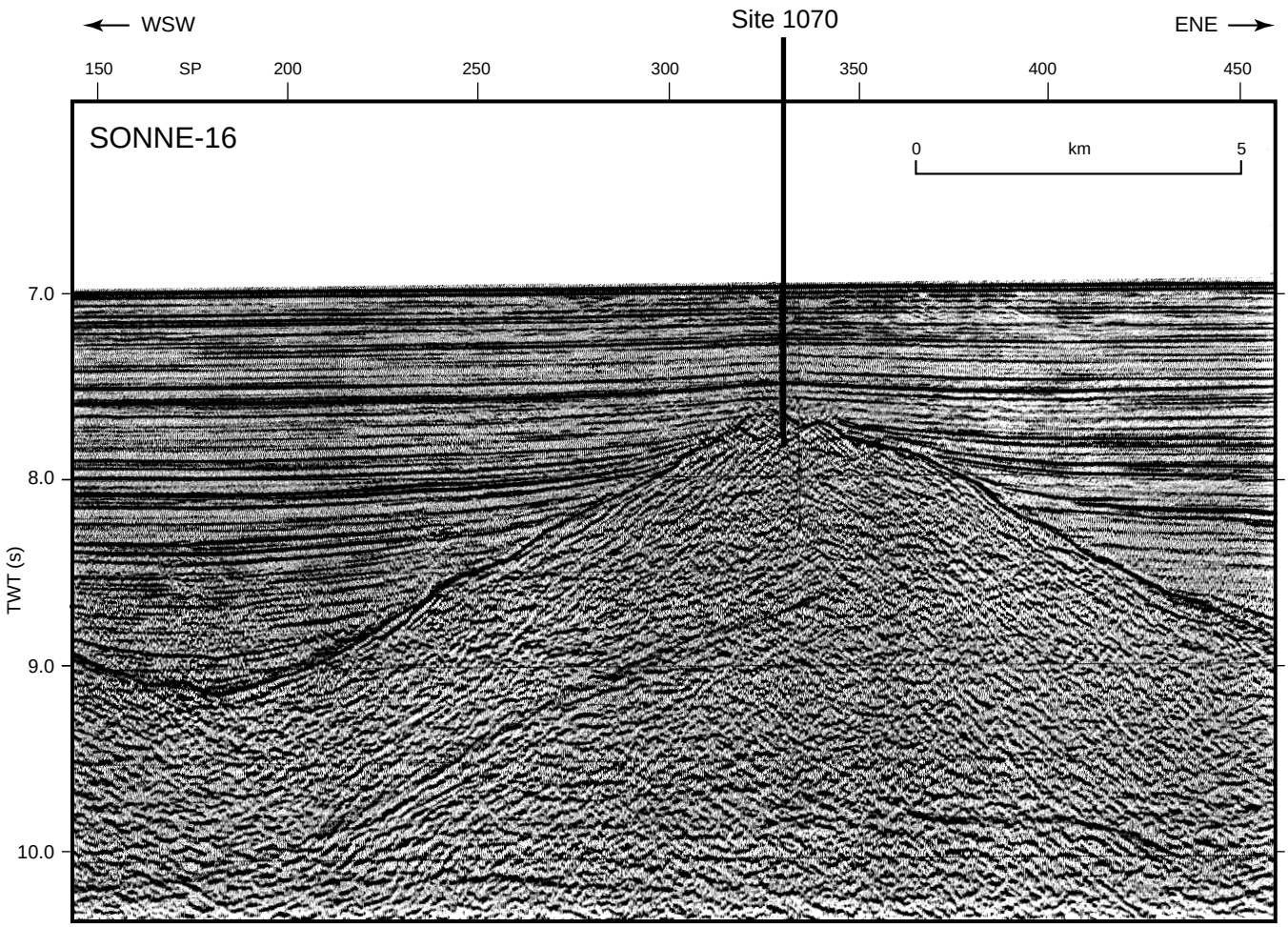

Figure 4. Sonne-16 multichannel migrated seismic reflection profile across Site 1070 (processed by S. Pickup; courtesy of K. Hinz).

Table 1. Site 1070 coring summary.

Core	Date (June 1997)	Time (GMT)	Interval (mbsf)	Length cored (m)	Length recovered (m)	Recovery (%)
Drilled from 0.0 to 599.0 mbsf						
173-1070A-						
1R	03	0100	599.0-608.7	9.7	5.02	51.8
2R	03	0415	608.7-618.3	9.6	5.22	54.4
3R	03	0800	618.3-627.9	9.6	4.07	42.4
4R	03	1100	627.9-637.6	9.7	4.79	49.4
5R	03	1345	637.6-647.2	9.6	3.40	35.4
6R	03	1640	647.2-656.9	9.7	4.49	46.3
7R	03	2050	656.9-666.5	9.6	3.39	35.3
8R	04	0145	666.5-676.2	9.7	5.83	60.1
9R	04	0530	676.2-685.9	9.7	2.67	27.5
10R	04	0945	685.9-695.5	9.6	1.76	18.3
11R	04	1410	695.5-705.1	9.6	1.75	18.2
12R	04	1700	705.1-706.6	1.5	1.96	130.7
13R	05	0240	706.6-714.5	7.9	4.38	55.4
14R	05	0930	714.5-718.8	4.3	3.04	70.7
			Cored totals	119.8	51.77	43.2
			Drilled	599.0		
			Total	718.8		

An expanded version of this table with individual section lengths is on CD-ROM (back pocket, this volume).

overlain by nannofossil chalk, and which are capped by claystone. Some calcareous silty laminae occur at the base of these sequences. In Core 173-1070A-2R, pebble-sized pieces of calcareous sandstone, possibly part of upward-darkening sequences, occur between biscuits, and so may not be in their original position. The claystone in Core 173-1070A-3R is brown and contains black manganese(?)-rich streaks and sand-sized manganese(?) micronodules. A dolomitic silty chalk occurs in interval 173-1070A-3R-1, 64–70 cm, and, together with the overlying claystone, forms the lowermost upward-darkening sequence of Subunit IIC. The bioturbation intensity in Subunit IIC is probably high, but is only visible in the lighter colored intervals of the upward-darkening sequences.

Petrography

Smear-slide analyses reveal that the lithologies of the upward-darkening sequences contain similar mineralogic components to those observed at other Leg 173 sites. Clayey siltstones at the base of individual sequences are characterized by the abundance of quartz and common occurrence of feldspar, mica, and clay. Carbonate and accessory minerals are present at trace levels. The upper calcareous intervals are composed dominantly of nannofossils, plus abundant to rare quartz and carbonate minerals. The claystones at the tops of the sequences are slightly silty in most cases with this size-fraction dominated by quartz, feldspar, and mica.

Depositional Environment

The rationale for the interpretation of the upward-darkening sequences of Subunit IIC as calcareous turbidites overlain by hemipelagic clays, which is given in the site reports in the Leg 149 *Initial Re-*

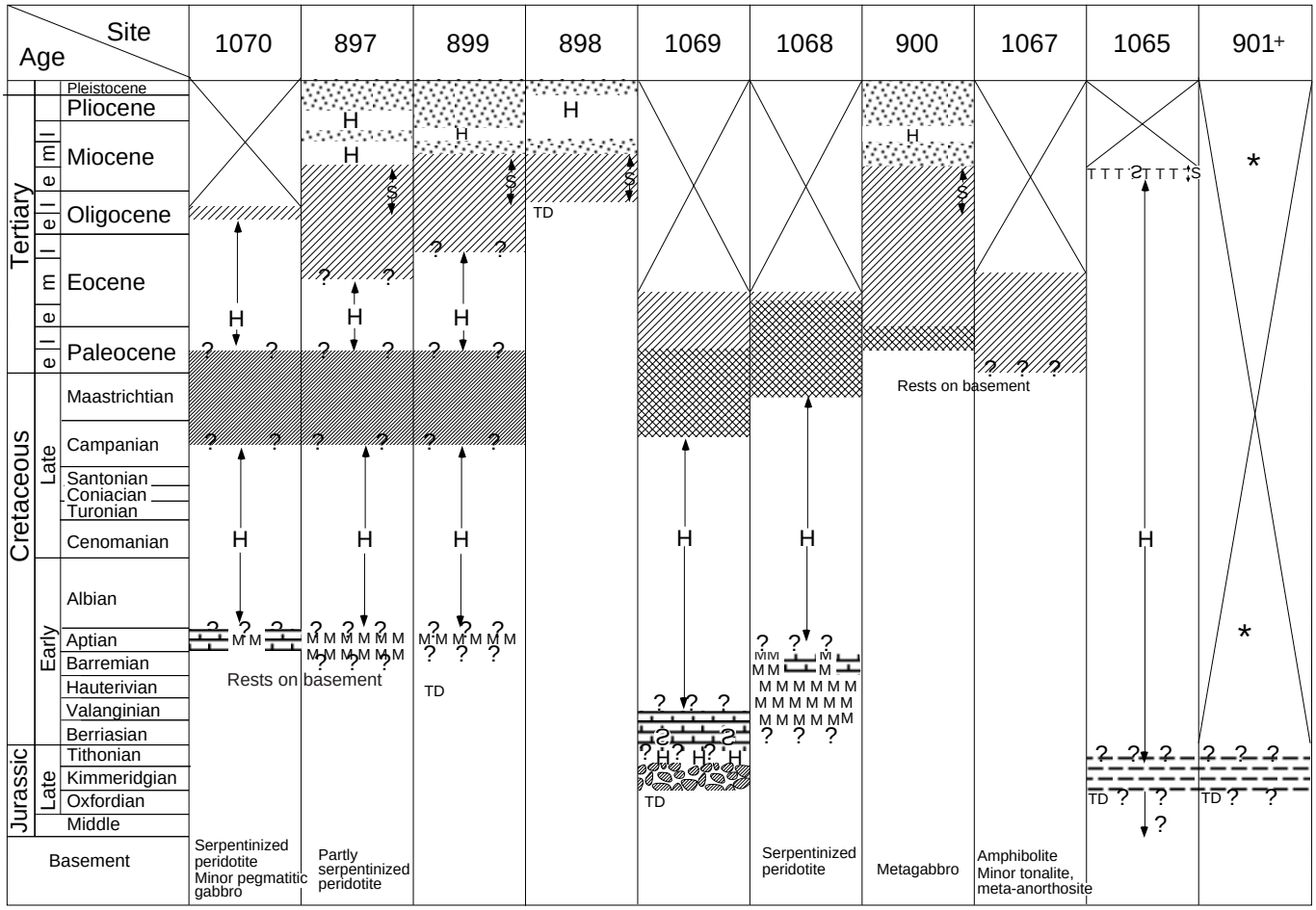

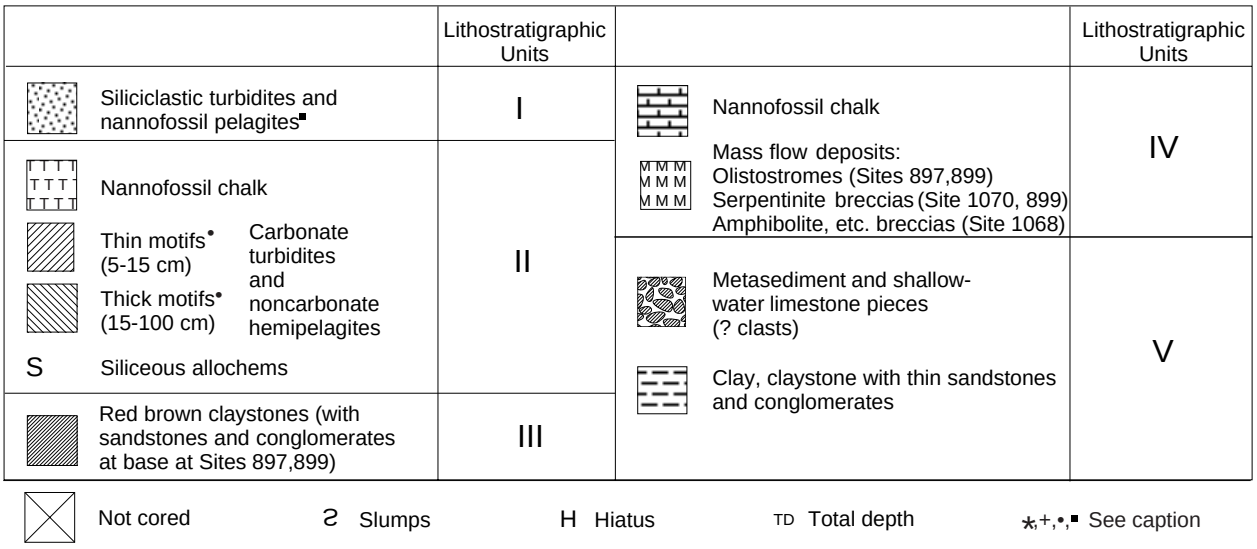

Figure 5. Simplified summaries of stratigraphic successions cored at Leg 149 and Leg 173 sites. Unit III is almost barren of fossils and so its age is uncertain. + = Unit V as shown in Site 901 was designated by Shipboard Scientific Party (1994d) as Unit II, following the normal ODP practice of numbering units sequentially downhole; * = a washed core recovered Miocene nannofossil ooze and a 5-mm-thick layer of gray clay of Aptian age. Solid square = nannofossil pelagites dominant at Site 900. Solid circles = "motifs" refers to types of upward-darkening sequences shown in Figure 3 of the "Site 1068" chapter and Figure 8 of the "Site 1069" chapter (both this volume). The cross-hatched symbols on the summary chart indicate that both thin (Motif 2) and thick (Motif 1) sequences are present.

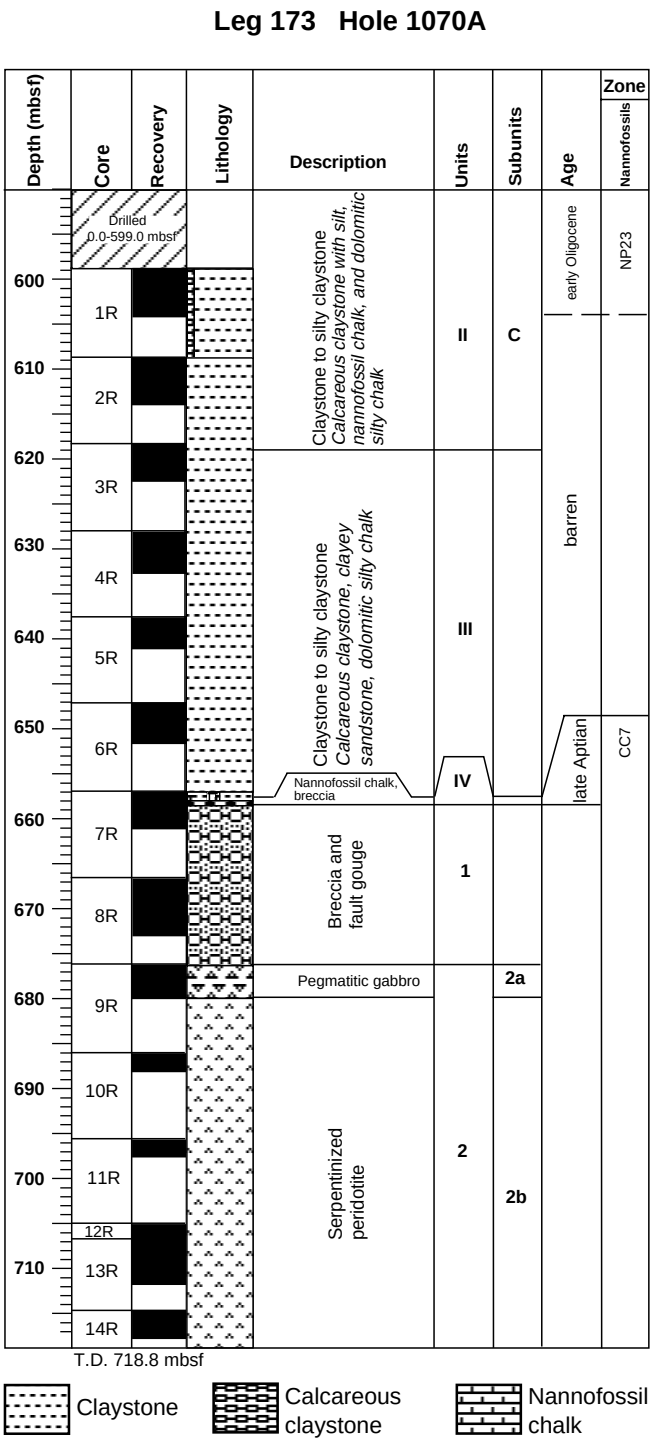

Figure 6. Summary lithostratigraphic column for Hole 1070A. Minor lithologies are listed in italics.

ports volume for Site 900 (Shipboard Scientific Party, 1994c), and the "Site 1067," "Site 1068," and "Site 1069" chapters (this volume), applies to the Subunit IIC sediments in Hole 1070A. The fact that the light colored, relatively coarse (silt to sand) calcareous base of individual upward-darkening sequences is typically absent or is limited to thin disturbed laminae at this site may be attributed to drilling disturbance, as some material may have been lost between biscuits, or may be a result of Site 1070 being further from the source area of the turbidites.

The dominance of hemipelagic clays in Subunit IIC in Hole 1070A could be explained by a decrease in the bulk sedimentation rate and an associated decreased turbidite input to this site compared to that at the sites to the east, or by post-depositional removal of the turbiditic calcareous fraction by dissolution because of prolonged exposure below the CCD.

Unit III

Interval: 173-1070A-3R-1, 70 cm, through 173-1070A-7R-2, 17 cm
Depth: 619.0–657.97 mbsf
Age: (barren) to late Aptian

General description

Recovery of Unit III over the 38.97-m cored interval ranged from 35% to 49%. The sediment is generally firm to hard, but moderate biscuiting obscures most of the internal structures and bedding relationships.

Claystone dominates the lithology of Unit III. In Section 173-1070A-6R-2 silty claystones to clayey sandstones occur. The claystones show a variety of colors, ranging from medium brown to light brown, yellowish gray, and moderate yellowish orange. The brown claystones commonly are mottled by manganese(?)-rich streaks and sand-sized micronodules of manganese(?). In interval 173-1070A-6R-2, 87–107 cm, thin beds and laminae of clayey sandstones, coarse sand- and gravel-sized clasts occur within the claystone (Fig. 7). One of the clayey sandstones is normally graded. Moderately bioturbated beds up to 5 cm thick occur in this interval. The brown claystone in interval 1070A-7R-1, 40–94 cm, reacts slightly with 10% hydrochloric acid.

Petrography

Smear-slide analyses of the claystones in Unit III show that minor amounts of quartz and mica and some carbonates occur in the silty fraction. Analysis by XRD of a thin light gray sandy interval in interval 173-1070A-6R-2, 39–41 cm, appears to be dominated by orthoclase and may contain ferro-manganese oxides (as Fe-Mn micronodules) or, less likely, magnetite. The presence of these minerals is consistent with high magnetic susceptibility and high natural gamma-ray activity measurements (see "Physical Properties" section, this chapter) made over this interval. One silty claystone at 173-1070A-5R-1, 1 cm, contains rare nannofossils (see "Biostratigraphy" section, this chapter). The remainder of Unit III is barren. Volcaniclastic particles, including altered vesicular ash and rare obsidian, and sand-sized mafic igneous minerals (e.g., olivine, plagioclase, biotite) and rock fragments were found in the coarse fraction of several samples from Core 173-1070A-5R to Core 1070A-7R (see "Biostratigraphy" section, this chapter).

Depositional Environment

The claystones of Unit III are interpreted as the product of slow accumulation of clay in an oxygenated environment on an abyssal plain below the CCD. The manganese content in the claystones and the micronodules, which occur in association with the accumulation of fish teeth (see "Biostratigraphy" section, this chapter), indicate a low depositional rate. The thin beds of sand in Section 173-1070A-6R-2 may have been deposited as turbidites (one is normally graded) and may be distal equivalents of the high-density turbidites present 20 km away at Site 897 (Shipboard Scientific Party, 1994a).

Table 2. Summary of lithostratigraphic Subunit IIC and Units III and IV at Hole 1070A.

Lithostratigraphic unit	Age	Thickness (m)	Major lithology, *minor lithology*	Color	Facies and *Environment/setting* (total meters described)	Intervals (mbsf)	Occurrence
IIC	early Oligocene	>20	Claystone to silty claystone >95% *Calcareous claystone with silt, nannofossil chalk, and dolomitic silty chalk <5%*	Various shades of brown and moderate reddish orange Greenish gray, light brown, and grayish orange	Carbonate turbidites and phyllosilicate clay hemipelagites *Abyssal plain, below/near CCD* (10.94)	Shallowest: 599.0 Base: 619.0	1R-1, 0 cm, to 3R-1, 70 cm
III	barren to late Aptian	39.57	Claystone to silty claystone >90% *Calcareous claystone and clayey sandstone, dolomitic silty chalk <10%*	Various shades of brown, moderate reddish orange, and yellowish gray Pale brown, grayish brown, and greenish gray	Phyllosilicate clay hemipelagites *Abyssal plain, below/near CCD* (17.12)	Top: 619.0 Base: 657.97	3R-1, 70 cm, to 7R-2, 17 cm
IV	late Aptian	0.4	Nannofossil chalk, calcareous chalk with nannofossils, and breccia 100%	Yellowish gray, moderate reddish orange, and light gray to white	Pelagites, turbidites, (?)debris flows *Abyssal plain, above CCD* (0.40)	Top: 657.97 Base: 658.37	7R-2, 17 cm, to 7R-2, 57 cm

Note: CCD = carbonate compensation depth.

Unit IV

Interval: 173-1070A-7R-2, 17 cm, through 173-1070A-7R-2, 57 cm
Depth: 657.97–658.37 mbsf
Age: late Aptian

General description

The boundary between Units III and IV is taken at the change from brown claystone to nannofossil claystone at interval 173-1070A-7R-2, 17 cm. The contact with the underlying basement Unit 1 occurs between Pieces 5 and 6 in Section 1070A-7R-2. Piece 5 consists of granule-sized altered basement clasts in a clayey matrix, and Piece 6 is composed largely of relatively coarse crystalline calcite, within which are scattered fragments of altered basement rocks. This is an abrupt change in lithology, and so we saw no reason to include the breccias that occur from Piece 6 in Section 7R-2 to Section 8R-5, 62 cm, as part of Unit IV. This abrupt change contrasts with the gradual downward increase in evidence for cataclasis and hydrothermal alteration that occurs in breccia Subunits IVB and IVC in Hole 1068A.

Unit IV is only 0.4 m thick and contains three lithologies: (1) an upper dark reddish gray and yellowish gray nannofossil chalk that occurs in interval 173-1070A-7R-2, 18–25 cm; (2) two intervals of small pieces (Pieces 2 and 6 in intervals 173-1070A-7R-2, 25–32 cm, and 55–57 cm) of coarse sand- to gravel-sized breccias that have an orange-brown calcareous clayey matrix, and (3) three pieces (interval 173-1070A-7R-2 [Pieces 3 through 5, 32–55 cm]) of interbedded reddish orange to moderate reddish brown calcareous chalk and breccias possessing a matrix of calcareous chalk. The top 1 cm of Piece 3 is finely laminated. The breccia bed in Piece 3 shows normal grading, and that in Piece 4 shows poorly developed normal grading overlain by inverse grading (Fig. 8). The breccias contain dark reddish brown, pale olive, and dark greenish yellow angular clasts of 1–8 mm in size, set in a light gray to white calcareous chalk matrix. Calcareous chalks containing scattered clasts occur adjacent to the breccias and vary in thickness between 1 and 4 cm.

Petrography

A thin section of the breccia and the calcareous chalk in Piece 4 shows that the clasts are completely altered to clay, and are cemented by coarse sparite. The lack of any contacts between the clasts indicates that a matrix-supported fabric must have existed originally, and that it was subsequently altered to sparite. The calcareous chalk above the breccia consists of elongate subrounded calcite grains ranging in size from 0.008 to 0.24 mm, but with the majority being between 0.04–0.07 mm. Light brown material of unknown composition occurs between the calcite grains. Upper Aptian nannofossils (see "Biostratigraphy" section, this chapter) are common in a smear slide of a sample of calcareous chalk taken beneath the breccia in 173-1070A-7R-2 (Piece 4).

Depositional Environment

The uppermost nannofossil chalk was deposited as pelagic sediment above the CCD. The parallel lamination in the upper part of the nannofossil chalk indicates some current action, but it is impossible to determine whether turbidite flow or contour currents were responsible. The matrix-supported breccias were probably deposited as small debris flows or turbidites transporting locally derived material relatively short distances. The petrographic features of the calcareous chalks interbedded with the breccias strongly suggest that their constituent calcite grains are largely detrital. The likely source of the calcite clasts is the underlying calcitized basement material of the type occurring in Core 173-1070A-7R-2 (Pieces 7 through 13; see "Igneous and Metamorphic Petrology" section, this chapter). The detrital calcite may have been transported by turbidity flow(s), but the presence of nannofossils indicates that some of the sediment is pelagic.

BIOSTRATIGRAPHY

Compared to other sites drilled in this area, Site 1070 was located in deeper water and farther from turbidite sources. Consequently, the cores recovered more hemipelagic sediments and less carbonate than in equivalent sections at the other sites (see "Lithostratigraphy" section, this chapter) and calcareous fossils were recovered only near the top (Paleogene) and bottom (Lower Cretaceous) portions of the cored sequence. There is a long barren interval in between (encompassing most of lithostratigraphic Unit III and Subunit IIC). Calcareous fossils at the top of the cored interval (lithostratigraphic Subunit IIC) were introduced primarily, if not exclusively, below the carbonate compensation depth (CCD) by turbidites. They contain significant amounts of reworked Eocene and Cretaceous materials, which renders biostratigraphic interpretations difficult. Calcareous fossils at the bottom of the cored section (lithostratigraphic Unit IV) are indigenous and were deposited above the CCD.

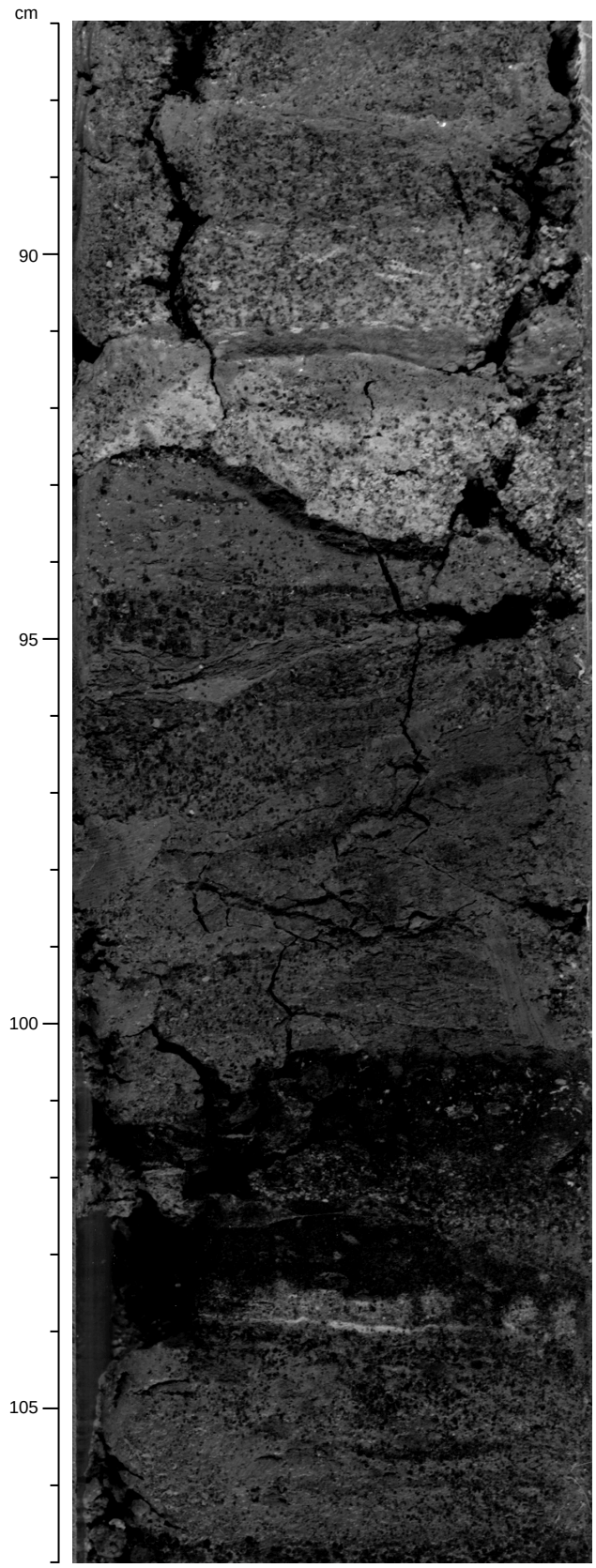

Figure 7. Core photograph of interval 173-1070A-6R-2, 87–107 cm, showing thin beds and laminae of clayey sandstones and coarse sand that occur toward the base of Unit III. The base of the light gray sand layer (~93 cm) is probably disturbed by drilling. The dark clayey layers in between 100.5–104 cm are bioturbated. The core is affected by moderate biscuiting.

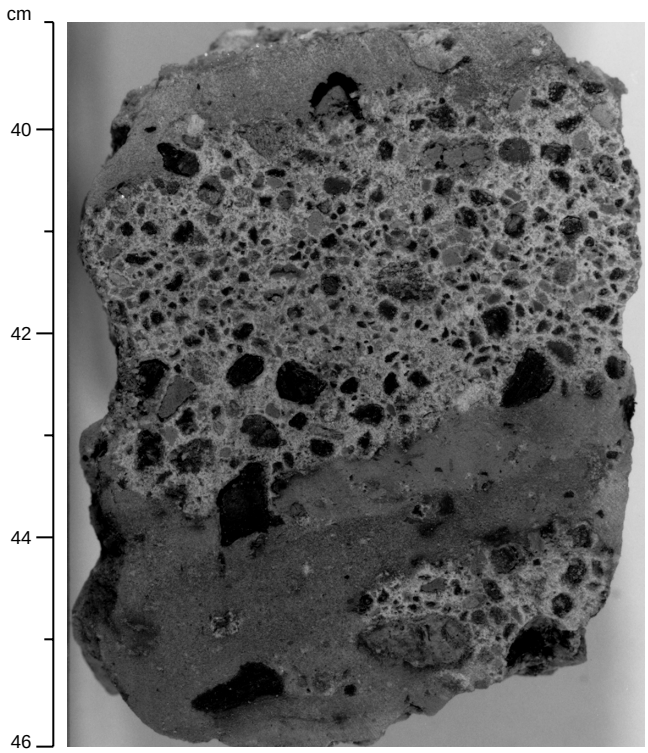

Figure 8. Core photograph of a breccia in Unit IV, interval 1070A-7R-2 (Piece 4, 39–46 cm). Poorly developed grading is present: normal toward the base, and inverse toward the top. The breccia matrix consists of sparite, and the angular to subrounded clasts are completely altered to clay.

Calcareous Nannofossils

As noted above, calcareous nannofossils were present only at the top and bottom of the recovered section. Sample 173-1070A-1R-1, 26–29 cm, from a greenish calcareous clay, was dominated by well-preserved *Cyclicargolithus floridanus* and large *Reticulofenestra stavensis* (up to 20 µm) plus *R. bisectus*, *Coccolithus pelagicus*, and *Discoaster tani nodifer* (many with prominent star-shaped central bosses). Abundant *Helicosphaera compacta*, *Sphenolithus predistentus*, and few *S. distentus* together suggest assignment to the lower Oligocene *Sphenolithus predistentus* Zone (NP23 of Martini, 1971). *Chiasmolithus altus* is also present but *C. oamaruensis* is not. Rare *Discoaster barbadiensis* and *D. saipanensis* are considered to be reworked from the Eocene.

Sample 173-1070A-1R-3, 15–16 cm, yielded a similar assemblage except no helicosphaerids were noted; *Reticulofenestra umbilica* and *Coccolithus formosus*, both lowermost Oligocene index taxa, were also absent. More reworked taxa were present in Sample 173-1070A-1R-4, 16–17 cm, including *Discoaster multiradiatus* from the Paleocene and *Prediscosphaera cretacea*, *Ceratolithoides aculeus*, and *Cribrosphaerella ehrenbergii* from the Cretaceous. Several specimens of *Coccolithus formosus*, along with rare *Discoaster barbadiensis* and *Reticulofenestra umbilica*, were also interpreted as reworked. *Helicosphaera perch-nielseniae* is present and is not known to range below Zone NP23, which is the age assigned to this sample. Section 173-1070A-1R-CC was sandy, poor in nannofossils, and contained several *Discoaster barbadiensis* (here considered reworked), and did not provide a reliable age determination.

The last sample downhole that contained Cenozoic nannofossils before the section became barren was Sample 173-1070A-2R-1, 9–10 cm. Compared to the assemblages described above, this one showed more evidence of dissolution. Several specimens of *Isth-*

molithus recurvus were noted, too many to be considered as reworked; thus, this sample was assigned to the lower Oligocene Zone NP22. Rare *Reticulofenestra umbilica, R. hillae, Coccolithus formosus, Discoaster barbadiensis,* and *D. saipanensis* are all considered reworked. If the latter two taxa are not reworked, then the sample is uppermost Eocene.

Nannofossiliferous samples were next encountered downhole near the base of lithostratigraphic Unit III. Although preservation is moderate because of dissolution and overgrowth, it is best in Sample 173-1070A-7R-1, 85–86 cm, which is from a brownish manganese-stained calcareous claystone. This and the assemblages investigated below in Unit IV are all assigned to the upper Aptian *Lithastrinus floralis* Zone (CC7). The assemblages are dominated by *Watznaueria barnesae* and contain common *Lithastrinus floralis* plus few to common *Hayesites irregularis,* rare *Corollithion achylosum,* and no *Micrantholithus hoschulzii* or *Nannoconus* spp. Forms that superficially resemble *Prediscosphaera columnata* are present, but these are interpreted as *Rotelapillus laffittei* overgrown by secondary calcite. A white chalk at interval 173-1070A-7R-2, 20 cm, contains a similar assemblage but is less well preserved because of in situ diagenesis. Below that, a pink matrix within a breccia contains many of the same elements, including *Lithastrinus floralis* and *Hayesites irregularis,* but in smaller numbers. A yellow paste within the breccia recovered from Sample 173-1070A-7R-CC is barren.

Planktonic Foraminifers

As mentioned above, calcareous microfossils are rare or more usually absent within thirty-five samples examined from this hole between Samples 173-1070A-1R-1, 43–48 cm, through 173-1070A-7R-CC. In Sample 173-1070A-1R-4, 22–25 cm, a fragment of *Globoquadrina* spp. was recovered, which suggests an age of Zone P21 (Oligocene or younger). Sample 173-1070A-1R-CC yielded two planktonic foraminiferal specimens of *Catapsydrax unicavus,* a long-ranging species with a stratigraphic distribution from late Eocene Zone P14 to early Miocene Zone N6, and one specimen of *Globigerinatheka* spp., which is characteristic of a late Eocene to early Oligocene assemblage. In Sample 173-1070A-3R-1, 64–69 cm, two very poorly preserved specimens of Paleogene aspect were recovered. One of these specimens is very tentatively identified as *Acarinina bullbrooki,* which, if identified correctly, would suggest an age for this sample within the range of late early Eocene (Zone P9) to middle Eocene (Zone P14). The remainder of the samples analyzed from Hole 1070A are barren of planktonic foraminifers.

Benthic Foraminifers

Calcareous benthic foraminifers occur sporadically in rare to common abundances in the material analyzed between Samples 173-1070A-1R-1, 43–48 cm, and 173-1070A-3R-CC. Below this, the remainder of the samples analyzed downhole to Sample 173-1070A-7R-CC are all barren of in situ calcareous benthic foraminifers.

Agglutinated benthic foraminifers occur consistently throughout the cored interval from Sample 173-1070A-1R-1, 43–48 cm, through Sample 173-1070A-7R-CC, with the exception of Sample 173-1070A-5R-CC, which is barren of foraminifers. Assemblages recorded are from the size fraction over 125 µm and include species such as *Glomospira* spp., *Ammodiscus* spp., *Bathysiphon* spp., *Hormosina* spp., and *Paratrochamminoides* spp. In Samples 173-1070A-4R-1, 11–16 cm, and 173-1070A-4R-4, 2–8 cm, the agglutinated foraminifers are stained brown. The washed residue volume of samples (i.e., total sediment above 63 µm) is very small for all material processed from Hole 1070A, between Samples 173-1070A-1R-1, 43–48 cm, and 173-1070A-7R-CC, which makes any interpretations based on quantitative analyses of agglutinated foraminifers less reliable.

Ichthyoliths occur persistently throughout Cores 173-1070A-1R through 6R and are of moderately high diversity both in size and shape, although no detailed analysis of their distribution has been done. Radiolarians occur rarely in Samples 173-1070A-2R-1, 6–9 cm, and 173-1070A-4R-4, 2–8 cm, and are abundant in Sample 173-1070A-3R-2, 61–65 cm. Although poorly preserved in the latter sample, the specimens are considered to be of early to middle Eocene age.

Other interesting features of the washed sediment residues include the first downhole occurrence of rare manganese in Sample 173-1070A-3R-3, 51–56 cm, and the common occurrence of botryoidal manganese in Samples 173-1070A-6R-1, 120–125 cm, 173-1070A-6R-2, 127–131 cm, and 173-1070A-6R-3, 18–22 cm. Small amounts of hematite are present in the washed residue from Sample 173-1070A-5R-1, 35–39 cm. Thin horizons of umber occur in Samples 173-1070A-6R-3, 18–22 cm, and 173-1070A-7R-1, 1–5 cm. Significant numbers of volcaniclastic sediment grains first occur downhole in Sample 173-1070A-5R-3, 29–33 cm, and are commonly found in samples downhole to Sample 173-1070A-6R-CC. Below this level in Core 173-1070A-7R, sedimentary residues are comprised of grains of a variety of igneous minerals.

The recovery of agglutinated foraminiferal assemblages characteristic of deep-water habitats and the paucity of sediment input of grain size larger than 63 µm suggests that the environment of deposition was probably at abyssal depths at least since Early Cretaceous times. The absence of radiolarians in the Cretaceous sediments suggests that the oceanic environment was not one of high productivity during the Mesozoic. During Paleogene times the preservation of calcareous microfossils possibly suggests deposition of pelagic sediments possibly above the CCD, but it is more likely that these microfossils were deposited below the CCD and protected from dissolution by rapid burial.

PALEOMAGNETISM

The archive halves of cores from Hole 1070A were measured at 5-cm intervals, using the pass-through cryogenic magnetometer. Sections were progressively demagnetized using peak alternating fields (AF) of 10, 20, 30, 40, 50, and 60 mT as described in the "Paleomagnetism" section, "Explanatory Notes" chapter (this volume). Fifteen discrete samples from sedimentary rocks were progressively AF demagnetized up to a peak field of 70 mT. In addition, six discrete samples from basement rocks and one sample from lithostratigraphic Unit III (see "Lithostratigraphy" section, this chapter) were thermally demagnetized to verify paleomagnetic reversals indicated by the pass-through measurements, to determine directional stability of the basement rocks, and to help identify the magnetic mineralogy of the recovered rocks. The volume magnetic susceptibility was routinely measured at 3-cm intervals on most of the cores from Hole 1070A as described in the "Physical Properties" section, "Explanatory Notes" chapter (this volume).

Magnetic Properties and Whole-Core Pass-Through Measurements

The NRM intensities and the magnetic intensities, after 60-mT AF demagnetization, are plotted in Figure 9. The NRM intensities for the basement rocks are mostly greater than for the sediments and average about 5×10^{-1} A/m. The sedimentary rocks from Site 1070 have been divided into three units (see "Lithostratigraphy" section, this chapter). The oldest unit, Unit IV is an Aptian nannofossil chalk and breccia unit (see "Biostratigraphy" and "Lithostratigraphy" sections, this chapter), that has an average NRM intensity of about 1.5×10^{-1} A/m. Unit III, a phyllosilicate clay, hemipelagite claystone to silty claystone, has an average NRM intensity of about 8.5×10^{-2} A/m. In Unit III at 650 mbsf, there is a hundred-fold decrease in magnetic intensity in Section 173-1070A-6R-3 (6.5×10^{-4} A/m). This decrease coincides with a change in lithology from moderate reddish orange claystone to greenish gray calcareous claystone (see "Litho-

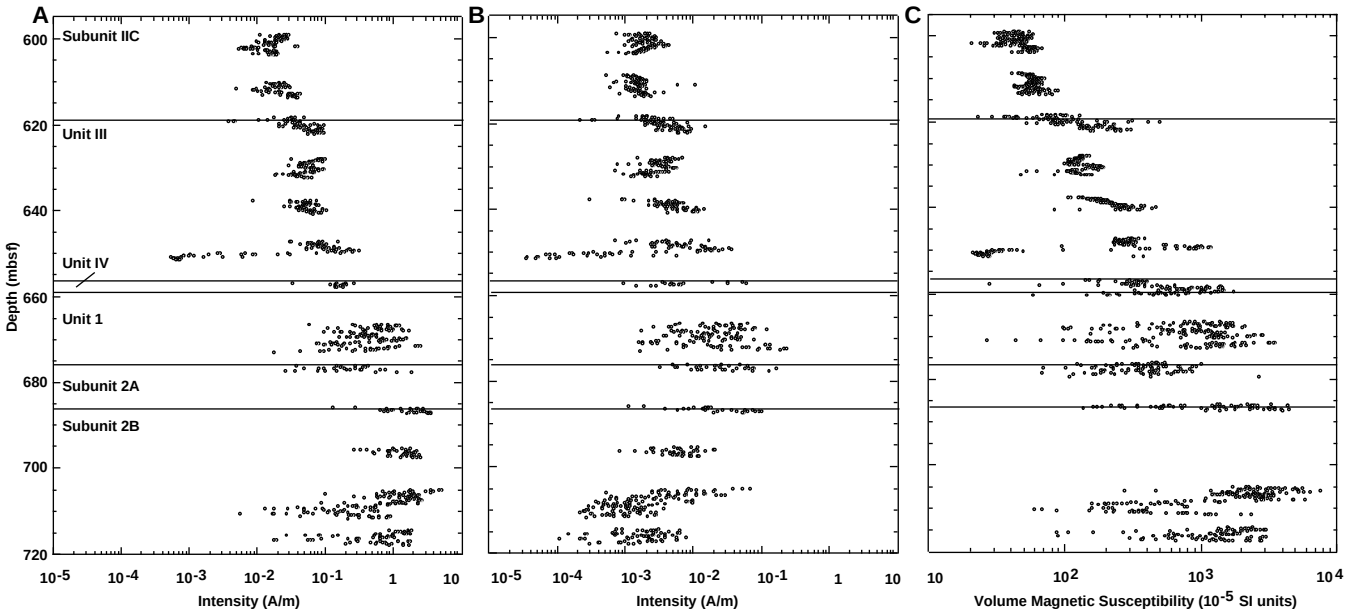

Figure 9. Plot of remanent intensity (**A**) before and (**B**) after 60-mT AF demagnetization and (**C**) volume magnetic susceptibility all as a function of sub-bottom depth in Hole 1070A. Upon demagnetization to 60 mT, a significant decrease in intensity and a shift of inclination toward negative values were observed, suggesting that drilling-induced magnetization is present. Horizontal axes are log scales.

stratigraphy" section, this chapter). The averaged NRM intensity for Subunit IIC, mostly a carbonate turbidite facies claystone to silty claystone, is about 1.5×10^{-2} A/m.

Variations in magnetic susceptibility generally parallel the variations in NRM intensity (Fig. 9). The magnetic susceptibility of sedimentary Subunit IIC is consistently low, averaging about 40×10^{-5} SI unit, concordant with the relatively weak NRM intensities observed in these cores. These values are confirmed by susceptibility measurements from 5 minicores used for demagnetization experiments. A general increase in susceptibility, observed within Core 173-1070A-3R at around 619 mbsf, coincides with the top of the Unit III (see "Lithostratigraphy" section, this chapter). In addition, there are significant susceptibility maxima and minima in Unit III at a depth of 650 mbsf (within Section 173-1070A-6R-2), with values greater than 1000×10^{-5} SI units (see Fig. 9). A close examination of the corresponding core reveals a transitional interval to a clayey sandstone and dolomitic silty chalk.

The magnetic susceptibility of the basement units is dispersed. The susceptibility of the basement units, however, is consistently above 150×10^{-5} SI units. The susceptibility maximum (>7000×10^{-5} SI units) occurs in the serpentinized peridotite of Subunit 2B (see "Igneous and Metamorphic Petrology" section, this chapter). This indicates that serpentinized peridotite may contribute significantly to the regional magnetic anomalies observed in the vicinity of Site 1070.

The NRM inclinations for the material recovered from Hole 1070A are strongly biased toward high positive values, with a mean >70° (Fig. 10). This value is significantly higher than the expected inclinations of about 60° for the present magnetic field and 40° for the Late Jurassic/Early Cretaceous field at Site 1070. This indicates that a pervasive remagnetization has been imparted by the coring process. Generally AF demagnetization removes the drilling-induced overprint. However, Figure 10 shows that AF demagnetization, up to 60 mT, is not always sufficient to remove this drilling-induced remagnetization component from the sediments if there is a significant amount of mechanical disturbance of the sediments (see "Paleomagnetism" section, "Explanatory Notes" chapter, this volume). This is demonstrated in Subunit IIC, where AF demagnetization treatment of up to 60 mT reduced the original NRM intensity by one order of magnitude, but resulted in virtually no change in mean inclination (Figs. 9, 10). However, AF demagnetization treatment to the 60-mT level is effective on the basement rocks. This is clearly shown in Figures 9 and 10 by large changes in inclination and intensity. The most noticeable changes occur in the serpentinized peridotite, Subunit 2B (see "Igneous and Metamorphic Petrology" section, this chapter). Different rock types acquire the drilling-induced magnetization to different extents and respond differently to AF demagnetization. This behavior suggests that there is a difference in the magnetic mineralogy and will be examined further in shore-based studies.

Alternating-Field and Thermal Demagnetization of Discrete Samples

Figure 11 shows examples of magnetic vector plots during AF and thermal demagnetization. There appear to be two overprints on the NRM of the samples. The most obvious one is the drilling-induced component characterized by inclinations greater than 75°. Generally, this component is most easily removed by AF demagnetization at 10 to 20 mT. The second overprint appears to be a viscous (VRM) component characterized by inclinations of 50° to 65°. Generally, thermal demagnetization at 150 to 200°C can isolate this component (see Table 3). The measured VRM may be useful for orienting the core for structural studies.

Judging from the spectrum of coercivity and unblocking temperature, it would appear that titanomagnetites are probably the main magnetic carrier in these samples. Because of the very limited number of shipboard study samples, this interpretation awaits verification ashore with more representative sampling, detailed rock magnetic measurements, and X-ray diffraction or other mineralogical identifications. It should be noted that the mean inclination values characteristic of the serpentinized peridotite cluster around 46°. This value, shallower than that of the present-day magnetic field of 59°, is similar

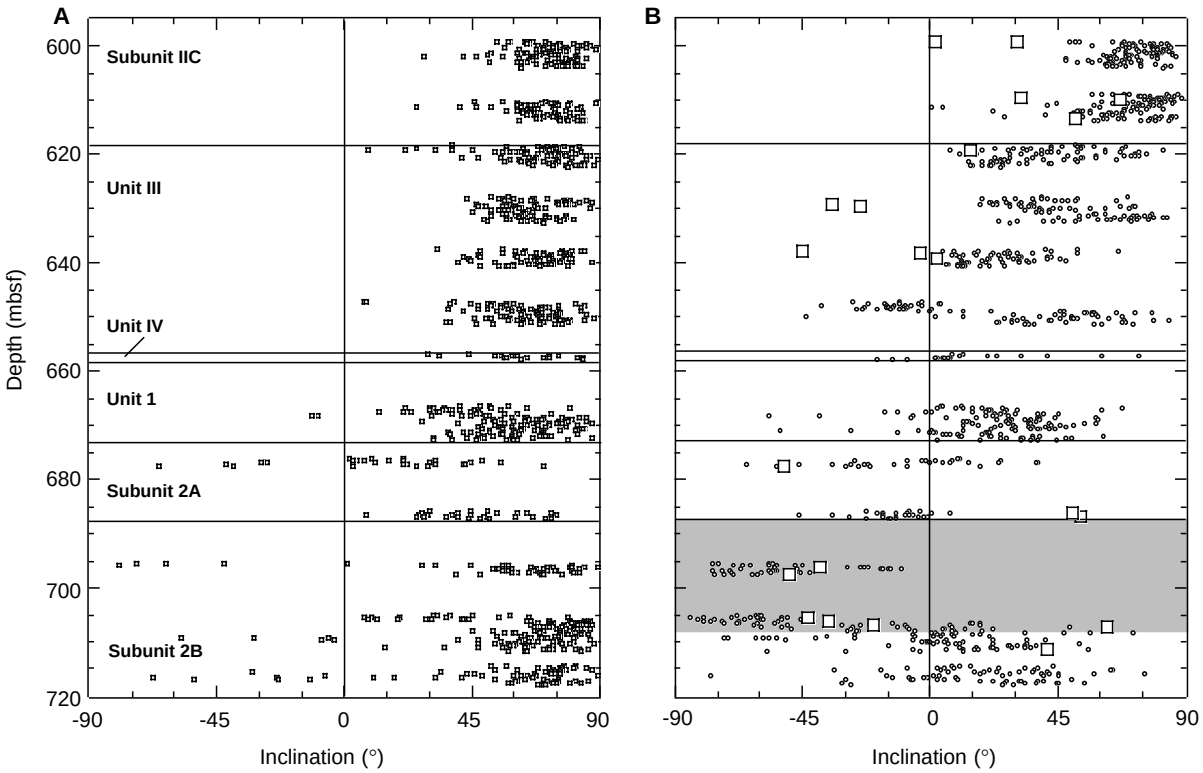

Figure 10. Downhole variation of magnetic inclination (**A**) before and (**B**) after 60-mT AF demagnetization for Hole 1070A. Discrete samples, taken from the center of undisturbed parts of the working-half section, are shown by large squares. Parts of the recovered core had a significant amount of mechanical disturbance of the sediments, thus AF demagnetization of the archive halves of cores was not always effective in removing the drilling-induced overprint (see "Paleomagnetism" section, "Explanatory Notes" chapter, this volume). Shaded area is the inferred reversed magnetic polarity zone within the serpentinized peridotites.

to the expected Cretaceous magnetic field for the Iberia Abyssal Plain.

Magnetostratigraphy

Results from the pass-through cryogenic magnetometer measurements and discrete sample demagnetization experiments indicate that 2 or 3 magnetic reversals may be recorded in this core, based on changes in sign of the magnetic inclinations (Cores 4R to 6R; 627.9–648.7 mbsf). Unfortunately, biostratigraphic data are not available for these cores, except to suggest that these reversals fall in a period between early Oligocene and Early Cretaceous. Shore-based biostratigraphic and isotopic studies as well as additional paleomagnetic samples from these intervals are needed to date and further characterize these reversals.

The most interesting result generated from the preliminary shipboard study is the identification of what appears to be a reversely magnetized zone in the serpentinized peridotites (Subunit 2B: see "Igneous and Metamorphic Petrology" section, this chapter). As shown in Figure 10, the inclinations in Cores 173-1070A-8R to 13R (667–715 mbsf) are stable and show a consistent polarity pattern in a depth zone of about 25 m. Within this zone, the magnetic inclinations of samples are predominantly negative (reversed polarity). In contrast, the magnetic inclinations of samples both above and below this zone are almost all positive (normal polarity). This same pattern, also found in the serpentinized peridotites recovered from nearby Leg 149 Sites 897 and 899 (Zhao, 1996), suggests that the Iberia Abyssal Plain peridotites preserve a Cretaceous magnetic record. Further analyses of this magnetic polarity zone, integrated with shore-based geochronologic and isotopic studies, may provide a unique opportunity for dating the tectonic processes that accompanied continental breakup and opening of the North Atlantic.

IGNEOUS AND METAMORPHIC PETROLOGY

Acoustic basement cored in Hole 1070A consists of breccia (Unit 1), which overlies pegmatitic gabbro and serpentinized peridotite (Unit 2). Breccia was encountered in Section 173-1070A-7R-2 at 658.37 mbsf, and rocks comprising Unit 2 were first recovered at the top of Section 173-1070A-9R-1 at 676.20 mbsf. The hole was terminated in serpentinized peridotite at 718.8 mbsf in Core 14R. Unit 2 has been subdivided into Subunit 2A beginning at 676.2 mbsf (pegmatitic gabbro) and the underlying Subunit 2B starting at 679.74 mbsf (mainly serpentinized peridotite). The average recoveries were 49.2% for Unit 1, 27.6% for Subunit 2A, and 39.2% for Subunit 2B.

Lithologic Description

The units and subunits defined for the acoustic basement are shown in Figure 12. Breccias comprising Unit 1 are overlain by Aptian sediments, which form the lowermost part of lithostratigraphic Unit IV above the acoustic basement (see "Lithostratigraphy" section, this chapter). The immediately overlying sedimentary rocks (Section 173-1070A-7R-2, 17–57 cm) are interbedded nannofossil chalks and breccias with nannofossil chalk matrices, containing coarse sand-sized clasts of serpentinite and calcite probably derived from the underlying breccia. The actual Unit IV/Unit 1 contact was

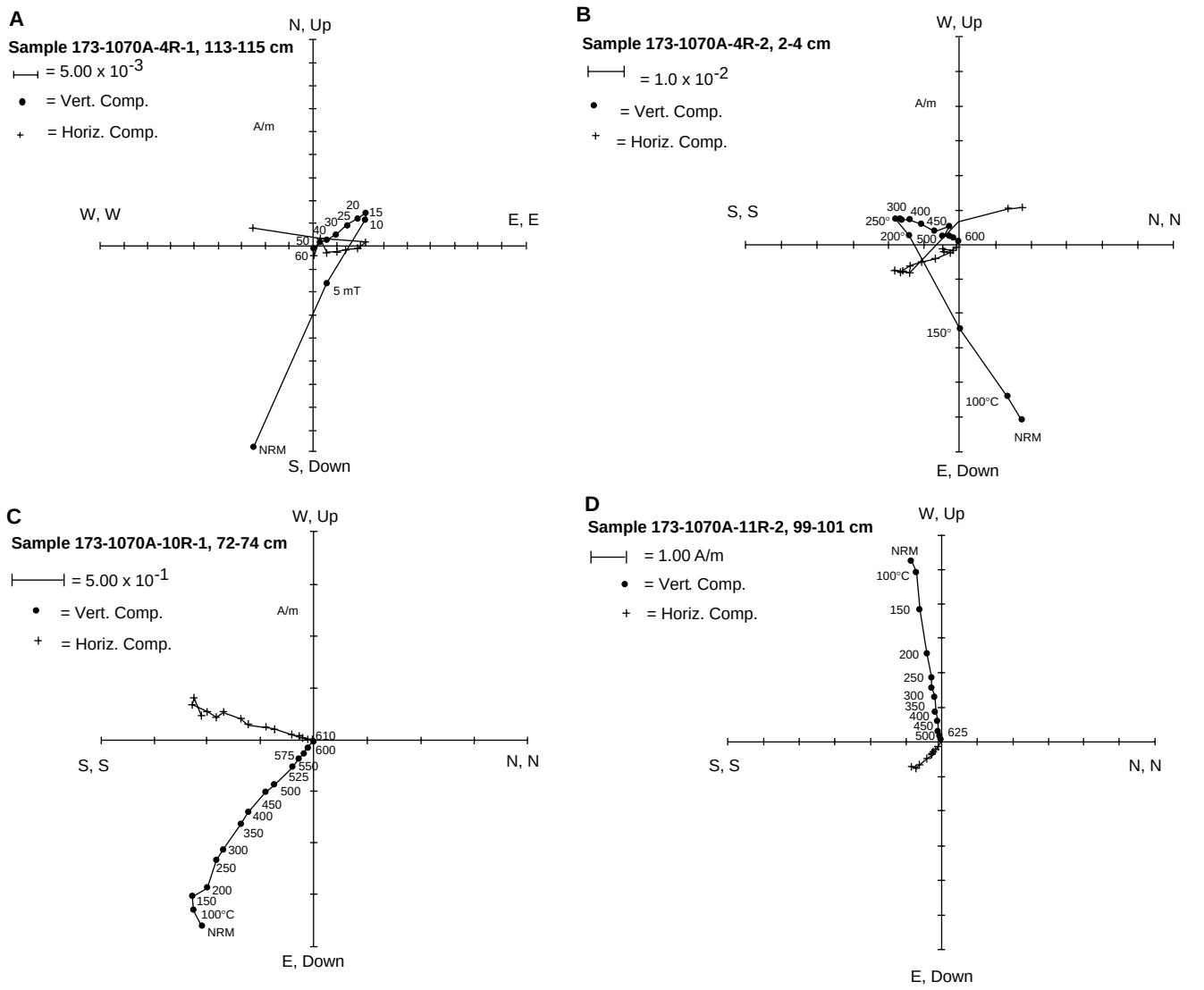

Figure 11. Representative vector end-point diagrams showing the results of (**A**) AF demagnetization for discrete Sample 173-1070A-4R-1, 113–115 cm, and (**B**) thermal demagnetization for Sample 173-1070A-4R-2, 2–4 cm (both samples are from Unit III), and (**C**) thermal demagnetization for serpentinized peridotite Samples 173-1070A-10R-1, 72–74 cm, and (**D**) 173-1070A-11R-2, 99–101 cm. Solid circles and crosses represent the projection of the magnetization vector end points on the vertical and horizontal planes, respectively. The declination values in this figure have not been corrected; see "Paleomagnetism" section, "Explanatory Notes" chapter, this volume.

Table 3. Viscous remanent magnetization (VRM) component characterized by inclinations of 50° to 65°.

Core, section, interval (cm)	Depth (mbsf)	Demagnetization range	Declination (°)	Inclination (°)
173-1070A-				
9R-1, 130	677.50	200-300°C	158.6	61.9
10R-1, 72	682.62	100-150°C	263.7	60.4
10R-1, 95	686.85	200-300°C	145.6	61.1
11R-1, 71	696.21	400-450°C	337.7	52.7
11R-2, 29	696.89	10-25 mT	116.5	64.4
11R-2, 99	697.59		No VRM for this sample	
12R-1, 54	705.69	200-250°C	156.7	53.3
12R-2, 40	706.36	500-525°C	155.4	51.3
12R-2, 83	706.79	5-10 mT	156.0	76.9
13R-1, 50	707.10	150-200 mT	191.0	62.5
13R-4, 68	711.25	200-250 mT	42.3	72.9

Note: Generally, thermal demagnetization at 150° to 200°C isolated the VRM component. The measured VRM may be useful for orienting the core for structural studies.

not preserved in the core. The matrix of the breccia of Unit 1 consists of relatively coarse-grained granular calcite and calcite rosettes, making it quite different than the fine calcite matrix in the nonmetasomatized and undeformed parts of the breccias found in Hole 1068A (see "Lithostratigraphy" section, "Site 1068" chapter, this volume); for this reason, and because the genesis of the breccia is at this stage uncertain, the breccia in Hole 1070A is not designated as a sedimentary unit (see also "Lithostratigraphy" and "Structural Geology" sections, this chapter).

The base of Unit 1 is marked by sheared serpentinite and possible fault gouge; the core recovery was poor and drilling disturbance is likely (interval 173-1070A-8R-5, 63–79 cm). The top of Unit 2 is marked by a coherent sample of sheared serpentinite 2 cm in thickness, which makes up Sample 173-1070A-9R-1 (Piece 1, 1–3 cm), and this is followed by pegmatitic gabbro, which comprises the bulk of Subunit 2A. Subunit 2A continues to interval 173-1070A-9R-3, 66–73 cm, where the contact between serpentinized peridotite and

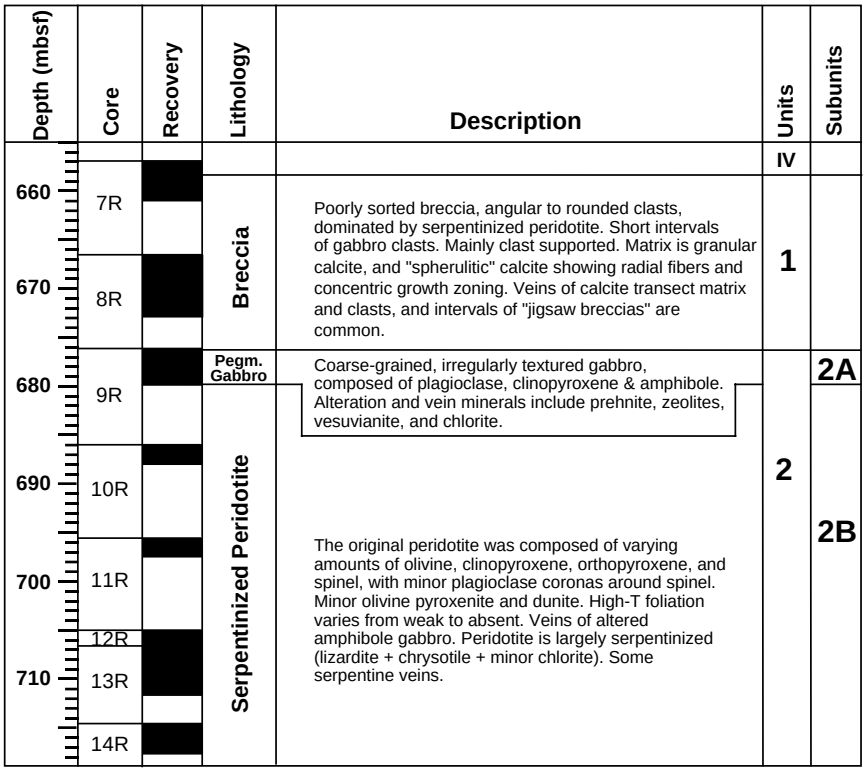

Figure 12. Summary of the lithologies composing the units and subunits of the acoustic basement in Hole 1070A.

Table 4. Lithologies of basement Unit 1 breccia, Hole 1070A.

Core, section, interval (cm)	Clasts (%)	Clast sizes (mm)	Clast type (%)	Clast shape	Veins
173-1070A-					
7R-2, 54-143	40	1-70	Serpentinite, calcite	Angular to rounded	
7R-3	50-70	1-130	Serpentinite 98	Angular to rounded	Calcite (rare)
7R-4	70	1-70	Serpentinite 95, gabbro 5	Angular to rounded	
8R-1	50-70	1-140	Serpentinite 95, gabbro 5	Angular to rounded, jigsaw	Calcite, some drusy
8R-2	50-70	1-150	Serpentinite 90, gabbro 10	Angular to rounded, jigsaw	Calcite, some drusy
8R-3	50-70	1-200	Serpentinite 95, gabbro 5	Angular to rounded, jigsaw	Calcite, some drusy
8R-4, 1-63	50-70	1-200	Gabbro 70, serpentinite 30	Angular to rounded, jigsaw	Calcite, some drusy
8R-4, 63-126	50-70	1-200	Serpentinite 95, gabbro 5	Angular to rounded, jigsaw	Calcite
8R-5	60	1-70	Serpentinite 100	Angular to rounded	Calcite

Note: Where no interval is listed, description refers to the entire section.

gabbro is visible in Piece 8. Serpentinized peridotite, with minor dikelets of altered gabbro, comprises Subunit 2B, in which the hole terminated at the base of Core 173-1070A-14R.

Unit 1 (Breccia)

Table 4 summarizes the main characteristics of the breccia. It consists of poorly sorted, angular to rounded clasts, dominantly of serpentinized peridotite, in a matrix of mainly calcite and minor limonite. The relative proportions of clasts and matrix are difficult to estimate, given the range in clast size and maximum diameter compared with the core width, but clast modes are mainly in the upper part of the range 40%–70%. Although clast support is considerably more common than matrix support, there are short intervals where the breccia appears to be matrix supported (e.g., interval 173-1070A-8R-1, 83–96 cm). In such cases the matrix mode is commonly obscured by the abundance of calcite veining. Serpentinized peridotite typically comprises more than 95% of the clasts, but in interval 173-1070A-8R-4, 1–63 cm, clasts of gabbro and plagioclase (either from anorthosite or coarse pegmatitic gabbro) are the more abundant. Rare clasts include calcite and one possible amphibolite. Calcite veining is common in Core 8R, either as constant-width veins that cut clasts and matrix alike or as irregular patches in the matrix. Areas of jigsaw structures, in which it appears that groups of clasts could be reassembled by removing the calcite veins and/or matrix, are abundant in Core 8R. The upper part of the breccia (interval 173-1070A-7R-2, 54–143 cm) is distinct in that small serpentinite clasts, commonly light greenish gray, are relatively more abundant, and “spherulitic” calcite showing radial fibers with concentric growth inclusions is quite common. Native copper veinlets cutting clasts or on stringers in the matrix were observed in Sample 173-1070A-8R-1 (Piece 2D, 130 cm). For further details and photographs of the breccia comprising Unit 1, see “Structural Geology” section, this chapter.

Subunit 2A (Pegmatitic Gabbro)

Subunit 2A is a very coarse-grained (pegmatitic) gabbro (Fig. 13). This subunit comprises all but the basal 20 cm of Core 173-1070A-9R; the upper boundary is at the top of Core 9R (676.20 mbsf), the base is at Sample 173-1070A-9R-3 (Piece 6), 679.74 mbsf. A total of

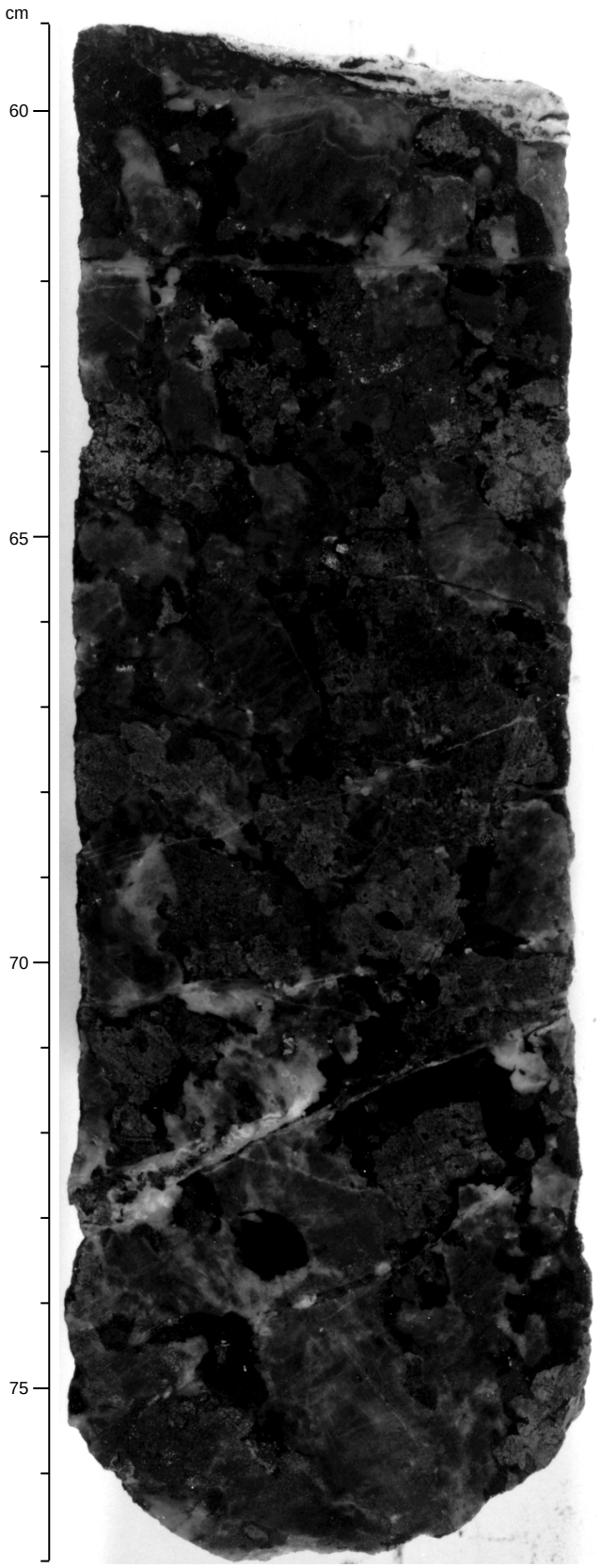

Figure 13. Relatively unaltered pegmatitic gabbro, composed of plagioclase (darker gray) and clinopyroxene (lighter gray), which has been largely enclosed and partly replaced by amphibole (black). Minor alteration is associated with fractures (interval 173-1070A-9R-2, 59–77 cm).

2.47 m was recovered. The top of the section appears to be in fault contact with the overlying breccia. At its base, the pegmatite appears to intrude serpentinite. A relatively fine-grained gabbro in contact with serpentinite in Core 9R-3 (Piece 8), may be a chilled margin.

The original igneous mineralogy of the pegmatite consists of plagioclase (40%–70%), amphibole (10%–25%), clinopyroxene (5%–50%), and ilmenite (1%–2%). A preliminary analysis of the scanned core images (420 cm^2 analyzed from Sections 173-1070A-9R-1 and 9R-2) suggests that amphibole + ilmenite in the core account for 33% of the mode. Plagioclase occurs as subhedral, tabular crystals 1–12 cm in maximum dimension. Throughout most of the pegmatite, plagioclase is the most abundant phase, usually comprising about 70% of the rock. Where fresh, the plagioclase is medium dark gray (N4). Most plagioclase shows the development of greenish to white (10G 6/2, N9) alteration rims that are most strongly developed in the vicinity of serpentine/calcite veins. The alteration assemblage includes sericite, chlorite, zeolites, and prehnite. Amphibole occurs in large (1–4 cm), anhedral, interstitial to poikilitic crystals. It often forms reaction rims surrounding both pyroxene and ilmenite. In hand samples, the amphibole has a reddish-bronze color on cut surfaces but is black on broken surfaces. It appears largely unaltered, even in samples where plagioclase and pyroxene have been virtually destroyed by alteration. Pyroxene occurs as light brownish-gray (5YR 6/1) blocky, anhedral crystals <1 to 4 cm in maximum dimension. In most samples, it composes less than 10% of the rock. However, the pyroxene mode may be as high as 50% in some very fresh samples (in particular, Sample 173-1070A-9R-2 [Piece 9]). In all samples, pyroxene is partially, or, more commonly, wholly rimmed and largely replaced by amphibole. Ilmenite occurs as relatively small (<1 cm) black crystals that occur as stringers or isolated pods. It can be recognized even in the most altered samples.

The pegmatitic gabbro is essentially undeformed and some portions (e.g., Sample 173-1070A-9R-2 [Pieces 9 and 10]) are relatively fresh. Most of the core, however, is moderately veined (veins 3%–5% by mode) by greenish veins. Some of these veins are calcitic, but others show little reaction with HCl and appear to be composed largely of silicate minerals. These may include chlorite, sericite, prehnite, zeolites, and serpentine.

In thin zones <2 cm in thickness, the pegmatitic gabbro appears to be locally affected by plastic deformation and shearing. This is manifested by flattening and elongation of plagioclase, ilmenite, and amphibole in the foliation plane (e.g., Sample 173-1070A-9R-1 [Pieces 3 and 5]). This deformation apparently involved local recrystallization of plagioclase and amphibole (see "Petrography" subsection) and was thus a high-temperature, possibly late magmatic deformation.

Subunit 2B (Serpentinized Peridotite)

The top of Subunit 2B is in Section 173-1070A-9R-3 (Piece 7) at 679.74 mbsf. Serpentinized peridotite was cored until the hole was terminated at the base of Core 14R at 718.8 mbsf. A total of 13.09 m of core was recovered over this 39.1-m interval. At its top, the serpentinized peridotite is intruded by the pegmatitic gabbro of Subunit 2B (see above). The base of the unit was not cored.

The serpentinized peridotite consists of 20%–95% (mostly 70%–95%, see below), mesh-textured serpentine and 5%–25% bastite. In many hand samples, a small amount of greenish primary orthopyroxene is visible in the cores of the bastites (e.g., Section 173-1070A-13R-4). Olivine, although not detected in hand samples, was found in several thin sections (e.g., Section 173-1070A-13R-CC, see "Petrographic Descriptions" subsection). A bright green serpentine mineral, although absent in most samples, is locally abundant (up to 70%, see below) and is interpreted as a replacement phase for clinopyroxene. Most serpentinized peridotite contains <1% Cr-spinel, although con-

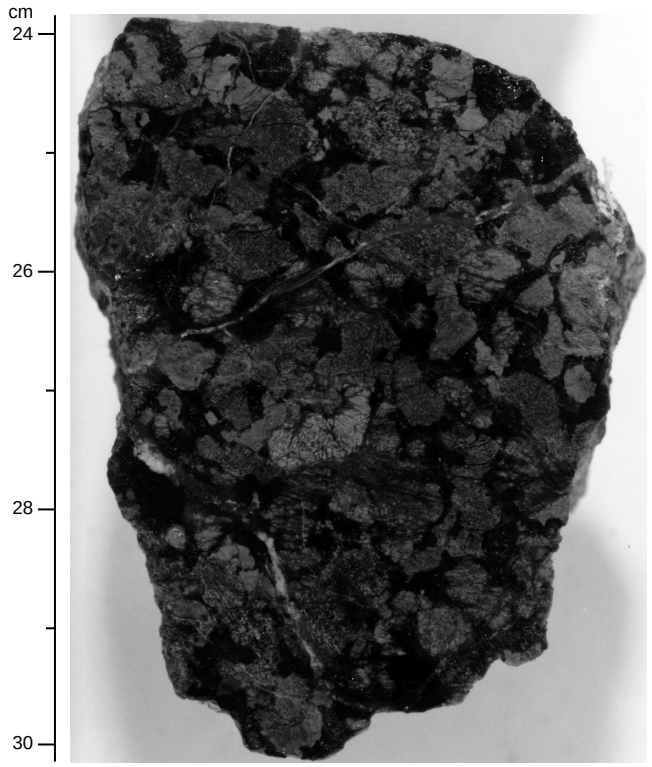

Figure 14. Partly serpentinized olivine pyroxenite. The olivine has been largely replaced by serpentine (black), while orthopyroxene has been largely, and clinopyroxene partly, altered to bastite pseudomorphs. Minor serpentine veins are present (interval 173-1070A-10R-2, 24–30 cm).

centrations of up to 3% occur in Sections 14R-2 and 14R-3. The spinel is rarely surrounded by haloes of chlorite (usually less than 1% of the rock), which may represent a replacement of original plagioclase.

For the most part, the peridotite protolith of the serpentinized peridotite contained 5%–30% orthopyroxene, 70%–95% olivine, and up to 10% clinopyroxene. Locally, pyroxene content was as high as 80% (e.g., Samples 173-1070A-10R-2 [Pieces 3, 5, 7, 8, and 9]), and about 5%–10% of the peridotite protolith can be characterized as an olivine pyroxenite (websterite; see Fig. 14). In several instances, especially in the olivine pyroxenites and in the other peridotites in Section 173-1070A-10R-2, a bright green serpentine making up 5%–25% of the peridotite (45%–70% of the olivine pyroxenite) is interpreted as a clinopyroxene replacement.

The serpentinite is intruded at several locations (e.g., intervals 173-1070A-11R-2 [Piece 5], and 13R-2 [Piece 1]) by strongly altered coarse-grained gabbroic dikes 1–4 cm thick (Fig. 15). Isolated pieces of gabbroic and feldspathic-rich rocks in the cores are interpreted as fragments of gabbroic dikes. The mineral assemblage in the dikes includes chlorite, serpentine, albitized plagioclase, sericite, talc, zeolite, and several unidentified, micro- to cryptocrystalline phases. Vesuvianite has been identified in thin section from Sample 173-1070A-11R-2 (Piece 5). Some ilmenite and amphibole has survived the otherwise pervasive alteration.

Veining is sparse, overall, in the serpentinized peridotite, ranging from 1%–5% of the rock. Veining is most intense in the vicinity of the dikes, where numerous serpentine(?) veins project at right angles from the altered gabbro into the serpentinized peridotite (Fig. 15; also

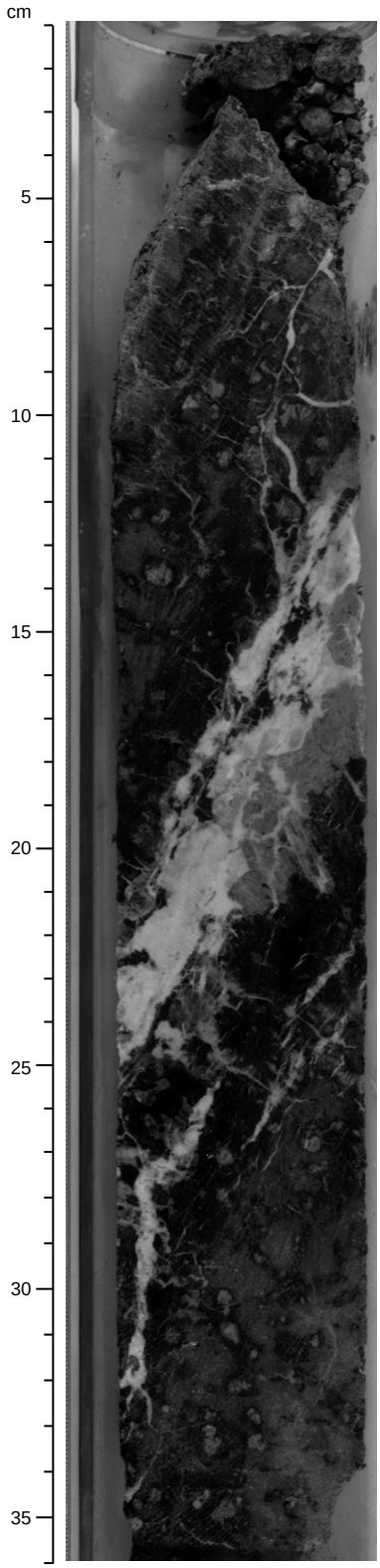

Figure 15. Amphibole gabbro dike in serpentinized peridotite. The peridotite has been largely replaced by serpentine, with pyroxenes being pseudomorphed by bastite. Relicts of amphibole are visible as the medium-gray material on the upper right of the vein, whereas the plagioclase has been largely replaced by chlorite, zeolites, talc, and serpentine (white material). Note the dark "blackwall" in the serpentinized peridotite adjacent to the vein, and thin veins of white serpentine both subparallel, and at a high angle, to the dike (interval 173-1070A-13R-2, 1–36 cm).

see "Structural Geology" section, this chapter). Other vein types include calcite (relatively rare) and serpentine.

Relicts of plastic deformation in the original peridotites are sporadically developed; many sections (e.g., all of Core 12R and the top two sections of Core 13R) appear undeformed. Local foliation, defined by the alignment of bastite pseudomorphs, is present in Core 11R, and in Sections 13R-2, 13R-3, 13R-4, and 14R-3 (see "Structural Geology" section, this chapter).

Petrographic Descriptions

In Hole 1070A, basement rocks consist of serpentinite breccia overlying pegmatitic gabbro and serpentinized peridotite including some pyroxenitic layers. Four thin sections document some of the petrographic characteristics of the clasts and the surrounding matrix present in the Unit 1 breccias. In the Unit 2 igneous rocks, two major petrographic subdivisions are recognized on the basis of mineralogy: pegmatitic gabbro (Subunit 2A) and serpentinized peridotite (Subunit 2B). Three thin sections were cut to describe the petrographic characteristics of the pegmatitic gabbro and one thin section documents the intrusive contact between the pegmatitic gabbro and the serpentinized peridotite. Nine additional thin sections were cut from the serpentinized peridotite and two from pyroxenitic layers (Table 5). Complete descriptions of the thin sections are given in Sections 5 and 6 (on CD-ROM, back pocket, this volume).

Unit 1 (Serpentinite Tectonic Breccia)

The breccia is largely clast-supported and only locally matrix-supported. The matrix in the thin sections represents 40% to 85%, whereas the clasts represent 15% to 60% of the rock and range in size from 0.1 mm to 2 cm (Fig. 16). Matrix calcite occurs either as granular aggregates or as grains showing radiating extinction. In some veins, the calcite grains occur as spheroidal aggregates of radiating fibers. The commonest clast present in Cores 173-1070A-7R and 8R is serpentinized peridotite with local occurrences of meta-anorthositic clasts or feldspar clasts from pegmatitic gabbro (Sample 173-1070A-8R-4 [Piece 1, 9–13 cm]).

Serpentinite Clasts

The serpentinized peridotite clasts are mainly composed of serpentine (75% to 100%), pyroxene (0 to 20%) and accessory spinel (<1% to 5%). Chlorite, tremolite, and opaque minerals (mainly magnetite) occur in variable abundances. Olivine is completely replaced by a serpentine mesh texture and veinlets of chrysotile crosscut the mesh texture. Magnetite replaces red-brown spinel in some clasts (Sample 173-1070A-11R-2 [Piece 5, 91–94 cm]). The clinopyroxene is relatively well-preserved when compared to the other original phases (e.g., Samples 173-1070A-7R-3 [Piece 1, 12–16 cm]; 8R-1 [Piece 2C, 48–52 cm]; 8R-4 [Piece 1, 9–13 cm]), but in some samples the clinopyroxene is replaced by bastite (Samples 173-1070A-7R-2 [Piece 9, 80–82 cm]; 8R-4 [Piece 6C, 118–118 cm]). Anhedral orthopyroxenes are totally replaced by bastite. Locally colorless to apple-green chlorite rims occur around spinel grains (Sample 173-1070A-10R-1 [Piece 10B, 137–138 cm]) or in veinlets. The chlorite surrounding spinel is interpreted as a replacement for plagioclase.

Gabbroic Clasts

The gabbroic clasts present in Sample 173-1070A-8R-4 [Piece 1, 9–13 cm], consist of 30% subhedral amphibole, 50% subhedral pla-

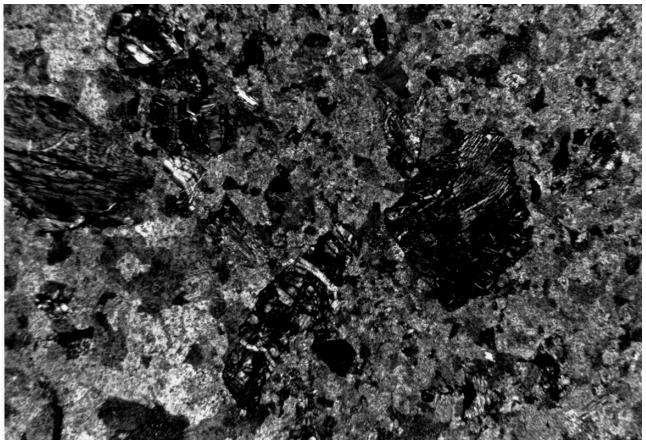

Figure 16. Photomicrograph of Unit 1 breccia showing serpentinite clasts in a calcite matrix (Sample 173-1070A-8R-4 (Piece 6, 115–118 cm); crossed polars).

Table 5. Hole 1070A rock types based on petrographic evidence.

Basement unit/ subunit	Core, section, interval	Rock name
	173-1070A-	
1	7R-2 (Piece 9, 80-82 cm)	Carbonate-rich breccia with serpentinized peridotite clasts
1	7R-3 (Piece 1, 12-16 cm)	Serpentinized peridotite
1	7R-3 (Piece 6, 89-93 cm)	Carbonate-rich breccia with serpentinized peridotite clasts
1	8R-1 (Piece 2C, 48-52 cm)	Serpentinized peridotite
1	8R-4 (Piece 1, 9-13 cm)	Carbonate-rich breccia with leucocratic metagabbro clasts
1	8R-4 (Piece 6C, 115-118)	Carbonate-rich breccia with serpentinized peridotite clasts
2A	9R-1 (Piece 2B, 18-22 cm)	Pegmatitic gabbro
2A	9R-2 (Piece 13, 103-106 cm)	Pegmatitic gabbro
2A	9R-2 (Piece 16, 122-125 cm)	Metamorphosed amphibole gabbro
2B	9R-CC	Serpentinized peridotite
2B	10R-1 (Piece 10B, 137-138 cm)	Serpentinized lherzolite
2B	10R-2 (Piece 9C, 77-81)	Partially serpentinized olivine pyroxenite
2B	10R-CC	Serpentinized peridotite
2B	11R-2 (Piece 5, 91-94)	Serpentinized peridotite/gabbro
2B	12R-2 (Piece 1A, 51-54)	Serpentinized plagioclase lherzolite
2B	13R-4 (Piece 4, 100-104)	Serpentinized lherzolite
2B	13R-CC	Serpentinized peridotite
2B	14R-1 (Piece 2B, 31-36)	Serpentinized harzburgite
2B	14R-2 (Piece 7, 96-98)	Leucocratic metagabbro
2B	14R-CC	Serpentinized peridotite

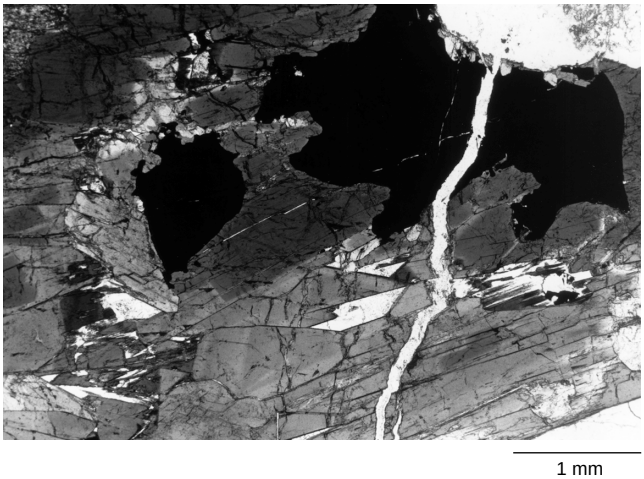

Figure 17. Photomicrograph of Subunit 2A pegmatitic gabbro showing zoned amphibole and ilmenite (opaque) cut by a thin zeolite vein (Sample 173-1070A-9R-2 [Piece 13, 103–106 cm]).

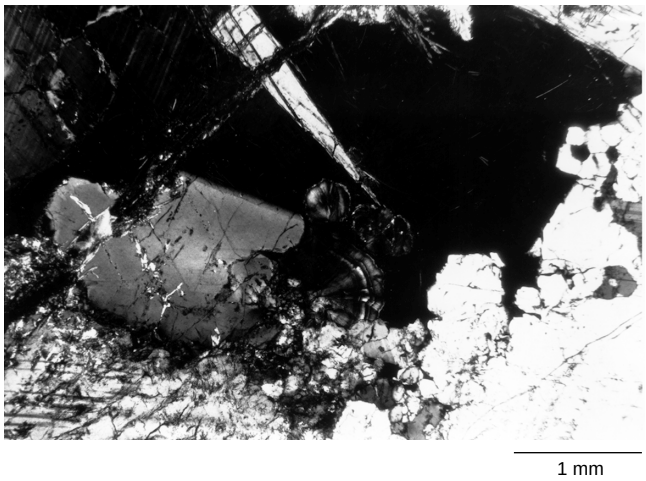

Figure 18. Photomicrograph of Subunit 2A pegmatitic gabbro showing nearly isotropic analcite (or wairakite), which has replaced plagioclase. Note recrystallization of plagioclase near the edge of the grain as a result of ductile deformation (Sample 173-1070A-9R-2 [Piece 13, 103–106 cm]).

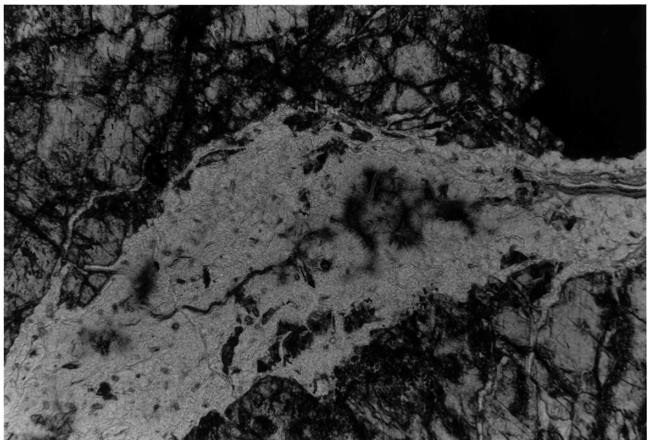

Figure 19. Photomicrograph of Subunit 2A hydrothermal veins filled with zeolite crosscutting the pegmatitic gabbro (Sample 173-1070A-9R-2 [Piece 16, 122-125 cm]). The dark material in the center of the vein may be green smectite.

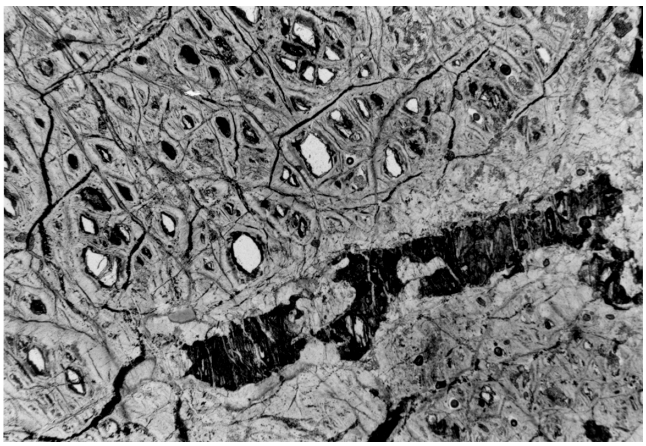

Figure 20. Photomicrograph of Subunit 2B serpentinized peridotite showing rare relicts of olivine and an elongate, interstitial partly altered clinopyroxene (Sample 173-1070A-13R-4 [Piece 4, 100–104 cm]).

gioclase, 15% colorless chlorite, and 5% sericite replacing former plagioclase.

Subunit 2A (Pegmatitic Gabbro)

The magmatic assemblage is well preserved in Sample 173-1070A-9R-2, Piece 2B, 18–22 cm, the rock exhibiting a very coarse-grained texture. The average grain size largely exceeds 3 cm, with some single grains up to 7 cm in length. This gabbro is made of 65% subhedral to anhedral plagioclase, 5% anhedral clinopyroxene, 5% ilmenite, and trace primary red biotite. Both clinopyroxene and ilmenite are included in anhedral red-brown amphibole, which accounts for 25% of the thin section. Zoned green to blue-green amphibole rims around the magmatic red-brown amphibole and clinopyroxene (Sample 173-1070A-9R-2 [Piece 13, 103–106 cm]; Fig. 17) are probably the result of retrograde metamorphism. Clinopyroxene is replaced by amphibole, and plagioclase is partially replaced by amphibole, albite, microcrystalline chlorite, and at least two types of zeolite. Ilmenite, which contains some hematite exsolution, is partially replaced by magnetite. The gabbro shows local shear zones that are associated with the development of blue-green amphibole and limited recrystallization of plagioclase (Fig. 18).

The late evolution of the gabbro took place under very low-grade conditions with the occurrence of zeolite at the expense of plagioclase and smectite at the expense of amphibole. This very low-grade metamorphic evolution is associated with veining (Sample 173-1070A-9R-2 [Piece 16, 122–125 cm]). There are probably several generations of veins. Alteration and vein minerals include vesuvianite, prehnite, chlorite, analcite or wairakite, and zeolite (Fig. 19; and Sample 173-1070A-9R-2 [Piece 2B, 18–22 cm]).

Subunit 2B (Serpentinized Peridotites)

The mantle rocks recovered in Hole 1070A are weakly foliated or unfoliated. In general, the peridotites are strongly serpentinized; relicts of olivine were observed in some samples but relicts of ortho-

pyroxene, clinopyroxene and spinels are relatively more common (Fig. 20). Red-brown to deep red spinels are less abundant than in Hole 1068A (see "Igneous and Metamorphic Petrology" section, "Site 1068" chapter, this volume) and are not elongated in a foliation plane, but they are coarser grained (up to 4 mm). Moreover, the spinel, when present, is very rarely surrounded by pseudomorphs after plagioclase. The serpentine displays common mesh textures and bastite pseudomorphs after pyroxenes. In addition apple-green chlorite patches and coronas surround bastite pseudomorphs. Deep green chlorite veinlets crosscutting the serpentinite are observed throughout the thin sections. Relicts of original minerals are more common toward the bottom of Hole 1070A. Olivine relicts show dislocation lamellae and some kink bands corresponding to high-temperature upper mantle deformation. Pyroxene (orthopyroxene and clinopyroxene), although in places kinked, is mostly undeformed. Pyroxene forms discrete layers of pyroxenite where weak foliation is present (Core 173-1070A-10R [Piece 2]) or diffuse pyroxene-rich zones in foliated samples (interval 173-1070A-10R-2 [Piece 9C, 77–81 cm]). Clinopyroxene shows irregular shapes and in some rocks clearly occurs as an interstitial phase (Fig. 20). Protolithic assemblages suggest that the peridotites were lherzolites, harzburgites, and dunites, grading locally into pyroxenites.

Within the serpentinites, several gabbroic veins (1–4 cm thick) display a mineralogy (red-brown amphibole and ilmenite) similar to the Subunit 2A pegmatitic gabbro, which intruded the serpentinized peridotite. Five clear igneous contacts are observed in Samples 173-1070A-11R-2 (Piece 5, 91–94 cm); 13R-1 (Piece 1, 10–24 cm); 13R-4 (Piece 1A, 33–40 cm); 14R-2 (Piece 1, 14–18 cm); 14R-3 (Piece 6, 83–87 cm). One isolated piece of gabbroic composition is also observed in 173-1070A-13R-3 (Piece 5, 42–50 cm). These gabbros are highly altered into low-grade to very low-grade assemblages including zeolite, vesuvianite, albite, hydrogarnet, chlorite, smectite, epidote, and carbonate. An intrusive contact between the gabbro and serpentinite (Sample 173-1070A-11R-2 [Piece 5, 91–94 cm]) shows a highly retrograded gabbro. Few relicts of magmatic red-brown amphibole, biotite, and ilmenite are preserved. Plagioclase is totally replaced by chlorite and zeolite. The blue-green amphibole is mainly retrograded into smectite, chlorite, albite, and magnetite. The peridotite is highly serpentinized with serpentine mesh texture replacing olivine and bastite pseudomorphs after pyroxene. Veinlets filled with chlorite mark the contact between the gabbro and the peridotite. In addition, gabbro contacts (e.g., Sample 173-1070A-11R-2 [Piece 5, 91–94 cm]) are invaded by serpentine veins and patches. This observation suggests that the serpentinization process operated at least in part after intrusion of the igneous mafic phase. A white metasomatic lithology (Sample 173-1070A-14R-2 [Piece 7, 94–103 cm]) composed of plagioclase, talc, zeolite (Fig. 21), chlorite, and sphene could be a highly altered leucogabbro.

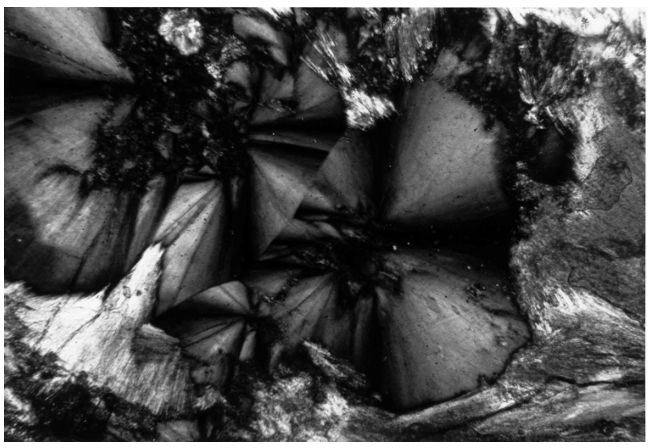

Figure 21. Photomicrograph of Subunit 2B of highly altered gabbroic veins in the serpentinized peridotite showing radiating clusters of fibrous zeolite minerals (Sample 173-1070A-14R-2 [Piece 7, 94–98 cm]).

X-ray Diffraction Studies

Diffraction spectra were collected from four rocks from Units 1 and 2 (Fig. 22). Three samples are from the matrix of Unit 1 (breccia), and one was collected from an altered, plagioclase-rich fragment (presumably part of a altered gabbroic dike) within the serpentinized peridotite (Subunit 2B). Small peaks attributable to serpentine were found in all samples (Fig. 22). The breccia matrix samples consist largely of calcite. Matrix Sample 173-1070A-7R-3, 110–111 cm, also contained minor peaks attributable to amphibole, chlorite, and goethite (Fig. 22C). The diffraction spectrum of the feldspathic Sample 173-1070A-14R-2, 93–95 cm, is dominated by sodic (albite to oligoclase) plagioclase. Small peaks attributable to serpentine and talc were also found. Other minor peaks were not identified.

The nearly pure calcite composition of the Unit 1 breccia matrix is consistent with petrographic and mesoscopic observations. Thus, the breccia matrix differs from that of the Hole 1068A samples where not only calcite is abundant, but albite, chlorite, and other minerals are important constituents of the breccia matrix (see "Igneous and Metamorphic Petrology" section, "Site 1068" chapter, this volume).

These differences between the breccias at the two sites appear to reflect differing modes of breccia formation. The Hole 1068A breccia appears to be a sedimentary rock, overprinted by tectonic and hydrothermal events (see "Igneous and Metamorphic Petrology" section, "Site 1068" chapter, this volume). On the other hand, the matrix of the Hole 1070A breccias appears to be composed of invasive, veinlike calcite and may reflect in situ, tectonic brecciation (see "Structural Geology" section, this chapter, for a more detailed discussion).

Major- and Trace-Element Geochemistry

Subunit 2B (Serpentinized Peridotite)

Four representative samples from the serpentinized peridotite and pyroxenite of Subunit 2B were chosen for shipboard whole-rock XRF analysis. The serpentinized peridotites (Samples 173-1070A-10R-1 [Piece 10A, 135–139 cm]; 12R-2 [Piece 1A, 51–56 cm]; and 13R-4 [Piece 4, 98–104 cm]) in general are comparable in chemical composition to the serpentinized peridotites of Holes 897C, 897D (Sawyer, Whitmarsh, Klaus, et. al., 1994), and 1068A that contain minimal plagioclase (Table 6; Fig. 23). The Site 1070 serpentinized peridotites have Mg-numbers of 92–94, which all fall within the range exhibited by the Hole 897C peridotites (Mg-numbers of 90–94) and the Hole 897D samples (Mg-numbers of 91–96). The serpentinized olivine pyroxenite (Sample 173-1070A-10R-2 [Piece 9A, 78–81 cm]) has a Mg-number of 91 but a significantly higher Cr content (6497 ppm; Table 6), which reflects the higher modal proportions of orthopyroxene and clinopyroxene (see "Petrographic Descriptions" subsection) compared to the serpentinized peridotites from this site (which have a Cr content of 1247–2275 ppm). The Site 1070 samples have TiO_2 abundances (0.21–0.34 wt%) that fall at the upper end of the range exhibited by the Site 897 and Site 1068 serpentinized peridotites, suggesting that before serpentinization the Site 1070 samples may have had larger amounts of clinopyroxene and orthopyroxene that were relatively high in TiO_2. If this interpretation is correct, significant CaO and Al_2O_3 must have been removed from the peridotites (see Table 6; Fig. 23). Compared to abyssal peridotites from the Mid-Atlantic Ridge (Leg 153; Cannat, Karson, Miller, et al., 1995), the Site 1070 peridotites have significantly higher TiO_2 contents but comparable MgO contents and slightly higher Mg-numbers (91.3–93.8; Fig. 23).

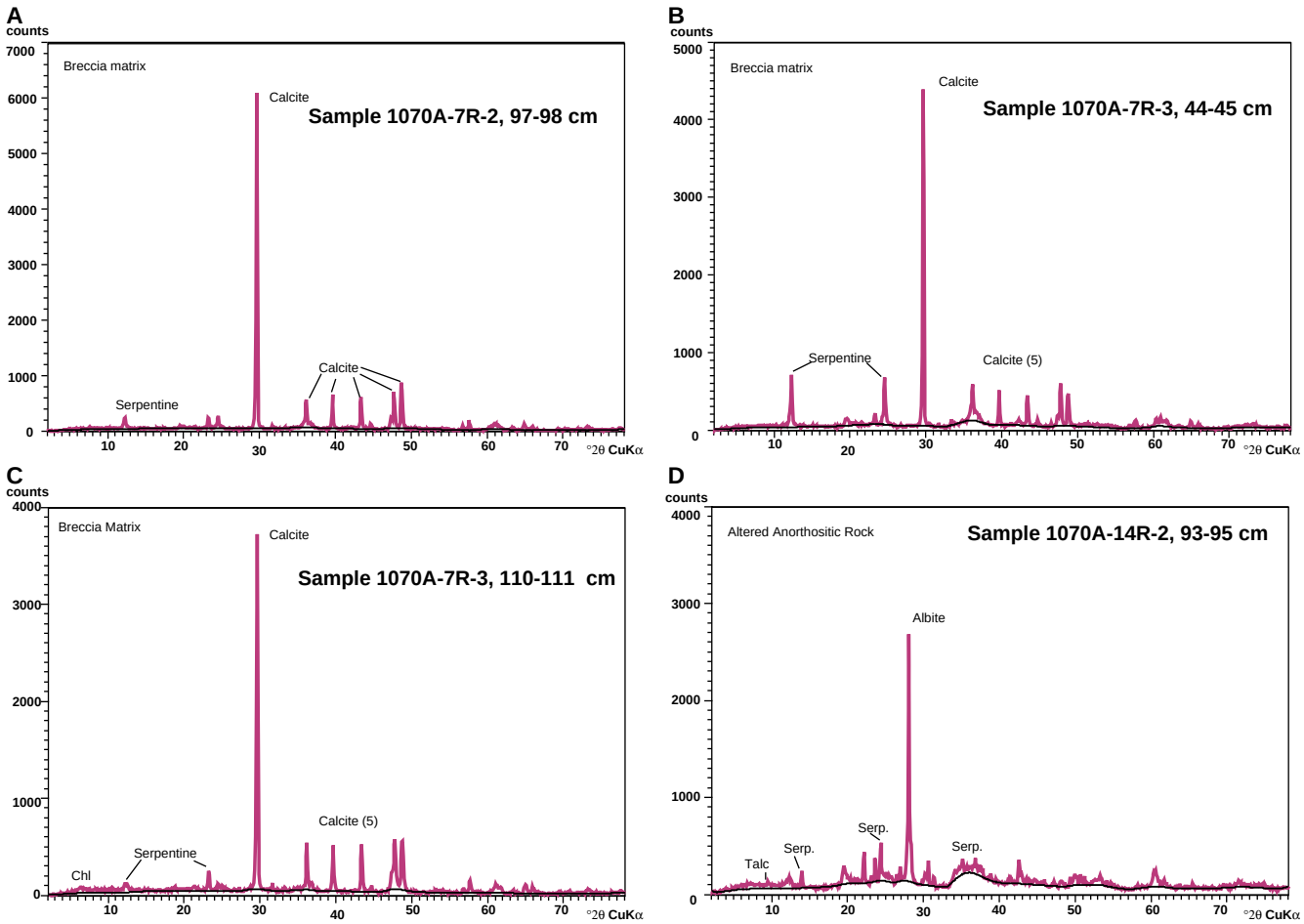

Figure 22. XRD patterns from the breccia matrix of Unit 1. **A.** Sample 173-1070A-7R-2, 97–98 cm. **B.** Sample 173-1070A-7R-3, 44–45 cm. **C.** Sample 173-1070A-7R-3, 110–111 cm. **D.** An altered leucocratic rock in Subunit 2B, Sample 173-1070A-14R-2, 93–95 cm. Serp. = serpentinite, chl. = chlorite.

STRUCTURAL GEOLOGY

Lithologies cored in Hole 1070A were (1) lower Oligocene to Cretaceous, poorly lithified claystones with variable, generally low calcite content (Units II and III; 599.0–657.97 mbsf), (2) upper Aptian chalk and sedimentary breccia, with graded bedding (Unit IV; 657.97–658.37 mbsf), (3) breccias of uncertain origin with "jigsaw" clasts, mostly of serpentinite, set in a calcite matrix (658.37–672.68 mbsf) underlain by fault gouge (672.68 to 676.2 mbsf), both belonging to Unit 1, (4) weakly deformed gabbro pegmatite (Subunit 2A; 676.2–679.74 mbsf) and (5) weakly deformed serpentinized peridotite with serpentine-rich veins and 1- to 5-cm-thick hydrothermally altered gabbro veins (Subunit 2B; 679.74–718.8 mbsf; see "Igneous and Metamorphic Petrology" section, this chapter). From a structural standpoint, two observations are of major interest: (1) the occurrence of a tectonized breccia and fault gouge separating undeformed sediments from weakly deformed gabbro pegmatites and serpentinized peridotites, and (2) the absence of a strong high-temperature deformation in the latter rocks, which represent unroofed mantle.

Units II and III: Sediments

No structural data were obtained from Units II and III because of strong drilling disturbance. A small normal fault was observed in interval 173-1070A-7R-1, 45–50 cm.

Unit IV: Breccia

Breccias of Unit IV are interbedded with nannofossil-rich chalk. Breccia beds are 3–4 cm thick and normally graded. Clasts of both sedimentary and igneous rocks occur, but serpentinized peridotite is dominant. Clasts are generally subangular and range in size from 2 to 10 mm. They are supported by a calcite-rich matrix. The bedding in the sedimentary breccia is shallowly to moderately inclined (two measurements: 18° and 27° dip with respect to the core's axis).

Unit 1: Breccia and Fault Gouge

Breccias of Unit 1 are typically characterized by <0.1 to 20 cm diameter clasts that are mostly (>90%) serpentinized peridotite and are supported by a matrix that is mostly calcite with <0.1 mm rock fragments. Other clast types include gabbro and anorthosite.

Clasts are everywhere "jigsaw" brecciated in three dimensions and on all scales. In several examples, it is possible to distinguish the margin of the former clast by piecing together a thin alteration rim (Fig. 24). Elsewhere in Unit 1, zones of monogenic clasts might represent more advanced jigsaw brecciation. This is particularly prevalent in Section 1070A-7R-3, where a zone of monogenic green serpentinized peridotite clasts occurs adjacent to a zone of monogenic pale vein serpentine clasts (Fig. 25). Although some intermingling of clasts occurs, this is restricted to a narrow (<1 cm) boundary layer.

Table 6. Major- and trace-element whole-rock compositions and CIPW norms for serpentinized peridotite and serpentinized pyroxenite from Subunit 2B, Hole 1070A.

Rock type:	Serpentinized lherzolite	Serpentinized olivine pyroxenite	Serpentinized lherzolite	Serpentinized lherzolite
Core, section:	10R-1	10R-2	12R-2	13R-4
Interval (cm):	135-139	78-81	51-56	98-104
Piece:	10A	9A	1A	4
Depth (mbsf):	687.25	688.10	706.47	711.55
SiO_2 (wt%)	45.85	44.50	43.53	43.24
TiO_2	0.29	0.34	0.22	0.21
Al_2O_3	1.61	6.00	2.01	0.57
Fe_2O_3	8.42	7.25	7.05	8.61
MnO	0.10	0.13	0.08	0.08
MgO	43.96	33.15	46.43	47.21
CaO	0.84	7.72	0.40	0.22
Na_2O	—	0.10	0.02	—
K_2O	0.07	0.06	0.05	0.04
P_2O_5	—	—	—	—
Total	101.13	99.24	99.77	100.18
Mg/(Mg+.86 Fe)	92.33	91.33	93.82	92.66
LOI	13.07	11.09	15.22	14.70
V (ppm)	54	362	50	17
Cr	2275	6497	1870	1247
Ni	2032	1757	1636	2201
Cu	6	168	5	4
Zn	43	44	37	40
Rb	0	0	0	0
Sr	14	22	9	9
Y	2	8	1	1
Zr	3	4	2	2
Nb	4	4	4	4
Ba	26	43	27	24
Ce	5	22	4	2
QZ	—	—	—	—
CO	0.01	—	1.2	0.13
OR	0.41	0.35	0.3	0.24
AB	—	0.85	0.17	—
AN	4.17	15.75	1.98	1.09
NE	—	—	—	—
DI	—	17.75	—	—
HY	29.31	9.57	19.43	16.78
OL	64.27	52.24	74.26	79.05
MT	1.71	1.48	1.44	1.75
IL	0.55	0.65	0.42	0.40
AP	—	—	—	—
Total	105.42	98.63	99.19	99.44

Note: Total iron is reported as Fe_2O_3. CIPW norms were calculated assuming Fe^{2+} = 0.86 Fe total. — = concentrations were below detection limit.

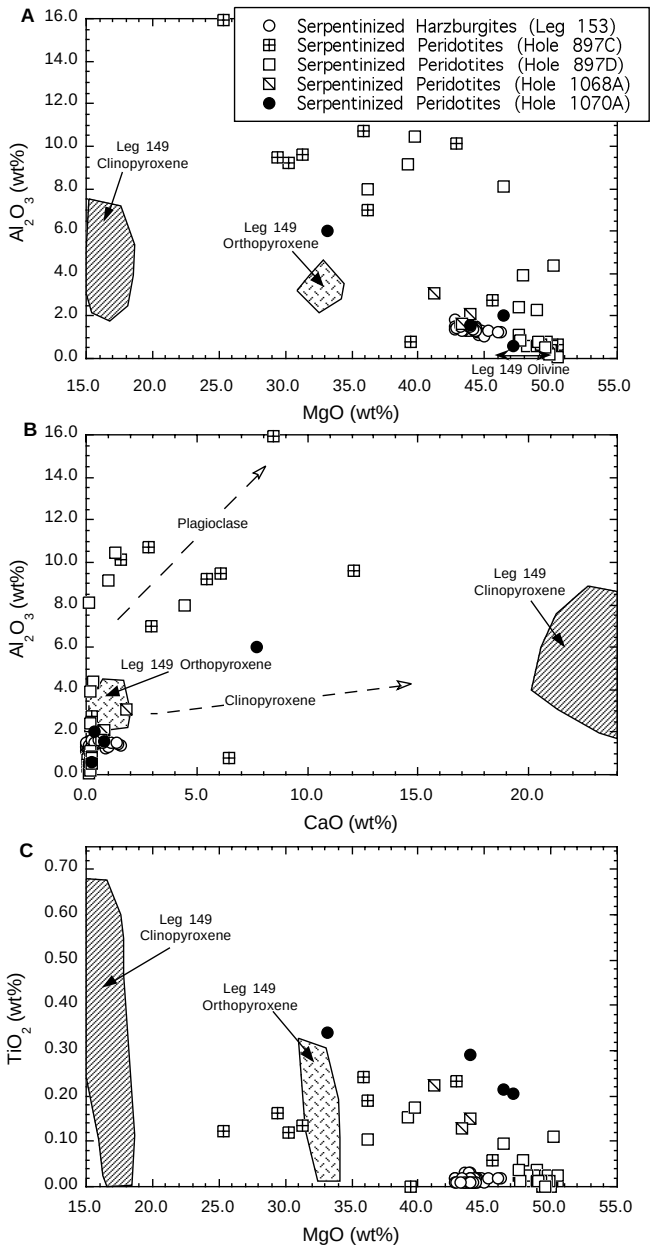

Figure 23. (**A**) MgO (wt%) vs. Al_2O_3 (wt%), (**B**) CaO (wt%) vs. Al_2O_3 (wt%), (**C**) MgO (wt%) vs. TiO_2 (wt%) variation diagrams for the Hole 1070A serpentinized peridotites. Also shown are the serpentinized peridotites from Holes 897C, 897D, and 1068A from the Iberia Abyssal Plain and Leg 153 serpentinized harzburgites from the Kane Transform region, Mid-Atlantic Ridge. Mineral compositional fields based on Leg 149 results are displayed. Data are from Sawyer, Whitmarsh, Klaus, et al., (1994); Cannat, Karson, Miller, et al. (1995); Cornen et al. (1996); Seifert and Brunotte (1996); and "Igneous and Metamorphic Petrology" section, "Site 1068" chapter, this volume.

The uppermost part of Unit 1 (interval 173-1070A-7R-2, 56–102 cm) is different from the rest of the breccia in that here the matrix-to-clast ratio is very high (more than 9:1). The rock consists essentially of calcite, most of which forms 1- to 2-mm-sized, radial-fibrous calcite spheroids (botryoidal calcite), visible as white spots in the core.

Throughout Unit 1, clasts are supported by a matrix of crystalline calcite and <0.1 mm rock fragments. Calcite occurs as (1) massive crystalline aggregates, (2) thin films that are optically continuous over 1–2 mm and surround rock fragments and clasts (Fig. 26), and (3) radiating fibers that form the discrete 1–2 mm spheroids mentioned above (botryoidal calcite; Fig. 27) or aggregates of partially formed smaller (0.2–0.5 mm) spheroids. Small calcite veins, which appear discrete from the matrix in hand specimen, are observed in thin section to be formed by similar aggregates of partially formed radiating spheroids. However, these are coarser (0.5–1 mm) and typically more complete (Fig. 28). Some large (1–2 cm) calcite veins contain vugs, which are lined with dog-tooth calcite (Fig. 29). Although some of these larger veins are transitional with the matrix, others clearly crosscut the matrix (Fig. 30). This observation suggests that some vein formation occurred after lithification. The mesh texture of serpentinite clasts is truncated by calcite veins and clast margins, indicating that the brecciation postdated serpentinization.

In general, the size of the largest clasts in each section increases downsection from Section 1070A-7R-2, 7 cm, to Section 1070A-8R-4, 20 cm, although reconstructed "jigsaw" clasts may have been significantly larger. An important exception to this general statement is

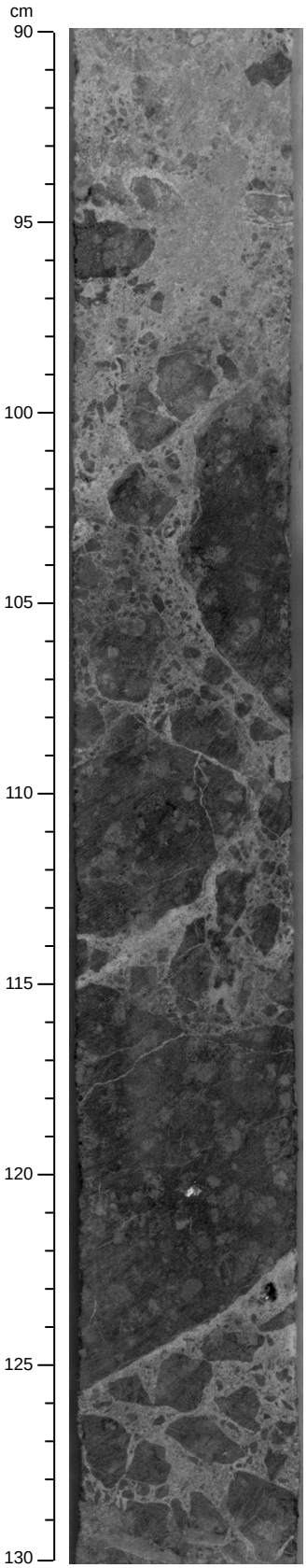

Figure 24. Jigsaw brecciated clast of serpentinized peridotite. Note pale fragmented rind at 99–102 cm and 129–130 cm on photograph (interval 173-1070A-8R-1, 90–130 cm).

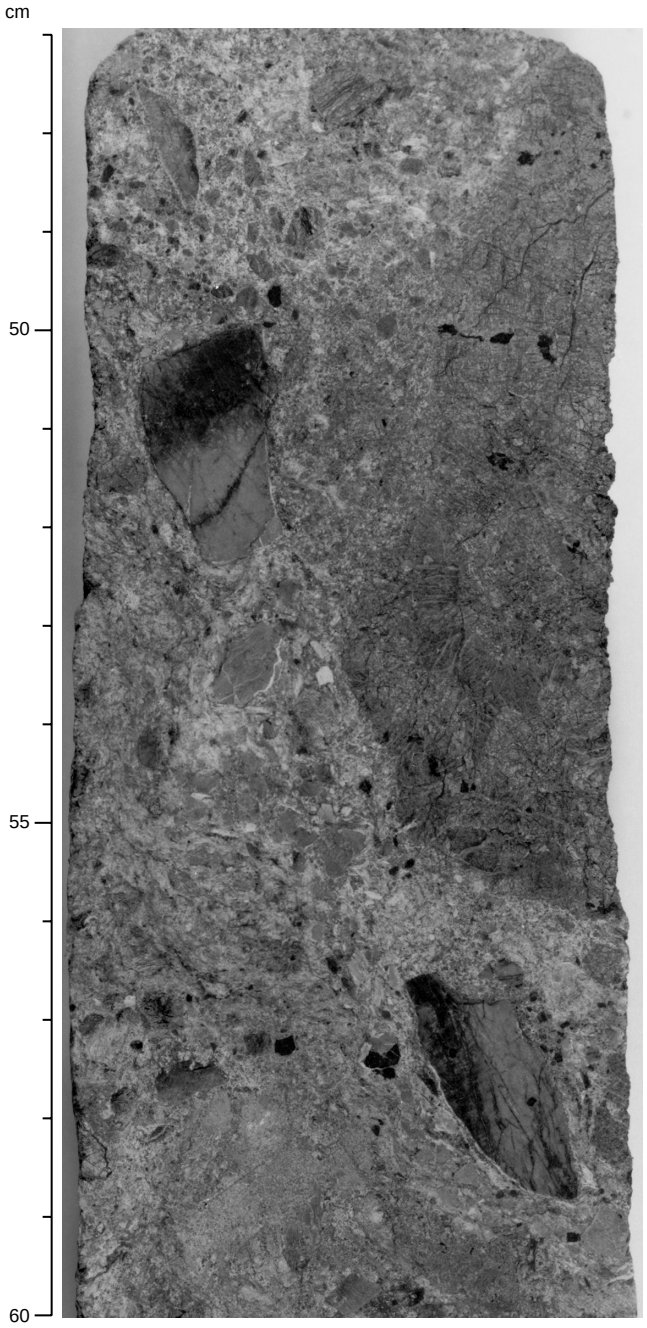

Figure 25. Zone of monogenic clasts of dark serpentinized peridotite (47–56 cm, right hand side of photograph) adjacent to a zone of monogenic clasts of pale vein serpentine (diagonal swath across photograph from 47–50 cm on the left-hand side to 56–59 cm on the right-hand side; interval 173-1070A-7R-3, 47–60 cm).

the lower part of Section 1070A-8R-5, where clasts are 0.1–5 cm in diameter. There is some indication that cataclasites, which are characterized by chloritization and millimeter-sized fragments occurring as discrete foliated bands, become more prevalent in this interval. It should be noted that the more general mechanism whereby clasts are "jigsaw" brecciated and then more pervasively fragmented is not cer-

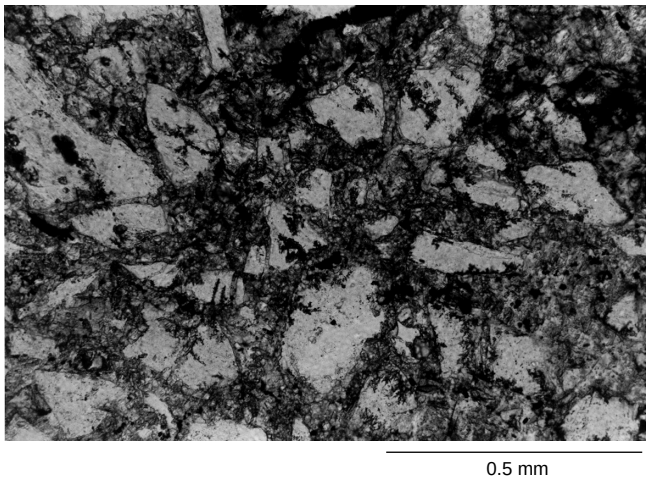

Figure 26. Photomicrograph showing grain boundary film of calcite in matrix-supported breccia (Sample 1070A-7R-2 [Piece 9, 80–82 cm]).

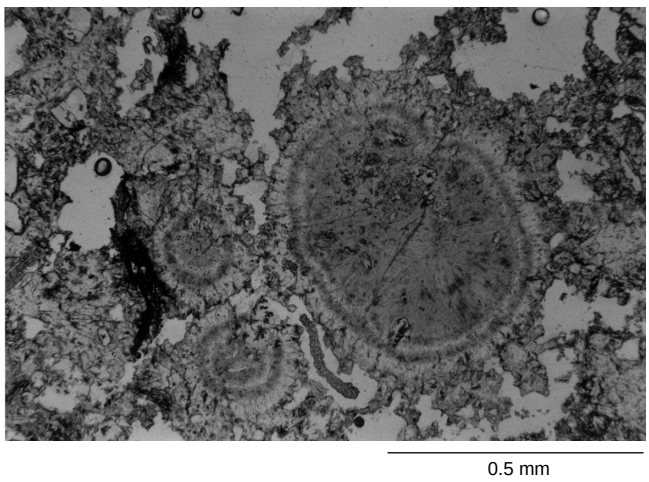

Figure 27. Photomicrograph showing distinct spheroids of radiating calcite fibers (Sample 173-1070A-7R-2 [Piece 9, 80–82 cm]).

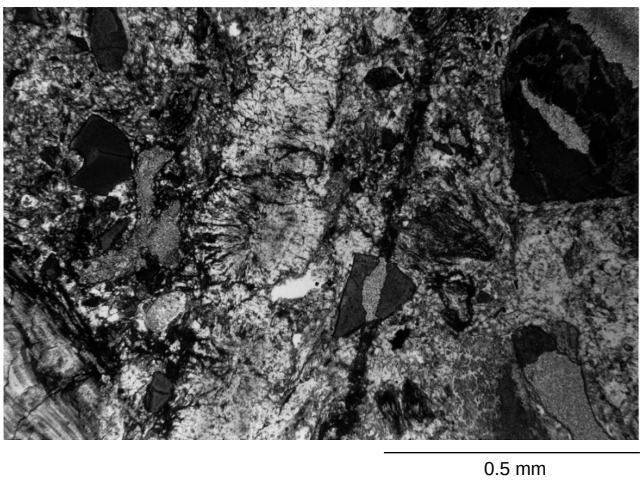

Figure 28. Photomicrograph showing vein filled by partially formed spheroids of radiating calcite fibers (cf. Figure 27; Sample 173-1070A-7R-3 [Piece 6, 89–93 cm]).

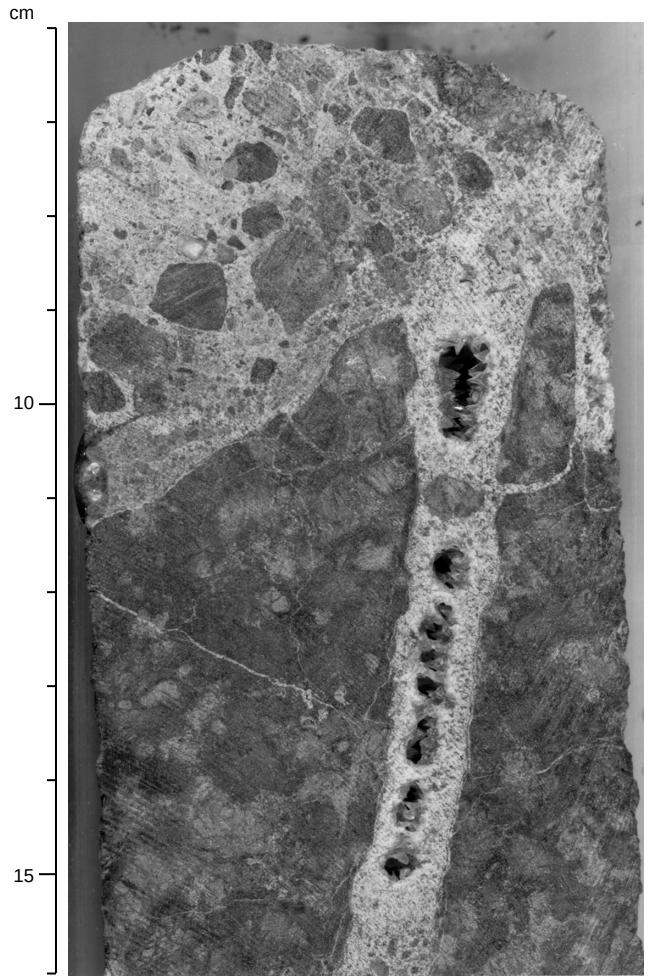

Figure 29. Vug filled with dog-tooth calcite (interval 173-1070A-8R-1, 6–16 cm).

tain, and might represent fluid-overpressuring and/or cataclasis. Toward the base of Section 1070A-8R-5, cataclasite grades into 10–15 cm of cohesive serpentine- and chlorite-rich fault gouge with 0.1–2 cm subrounded clasts of serpentinized dunite. At the base of Unit 1, there is 20 cm of incohesive serpentine- and chlorite-rich fault gouge with 1– to 3-mm rounded clasts of serpentinized dunite. At the top of Unit 2, there is 2 cm of chlorite schist with abundant 1– to 2-mm calcite veins. This probably records pervasive greenschist facies retrogression facilitated by deformation-assisted fluid infiltration along the fault gouge. Note that the downward succession, sedimentary breccia—tectonic breccia—fault gouge—basement rocks, and the increased cataclasis with depth in the breccia are similar to observations at Site 1068 (see “Structural Geology” section, “Site 1068” chapter, this volume).

Subunit 2A: Pegmatitic Gabbro

The pegmatitic gabbro is very coarse grained (2–3 cm) and shows only weak and heterogeneous deformation. In one thin section (Sample 173-1070A-9R-2, 103–106 cm), plagioclase shows undulatory extinction and a few deformation twins. Some plagioclase subgrains and polygonal, recrystallized grains (0.2 mm) occur along grain boundaries. Some large grains of brown amphibole are also strained (undulatory to patchy extinction), and locally small (0.1–0.2 mm),

Figure 30. Sketch showing calcite vein (in white) cross cutting already lithified matrix (interval 173-1070A-8R-2, 27–35 cm).

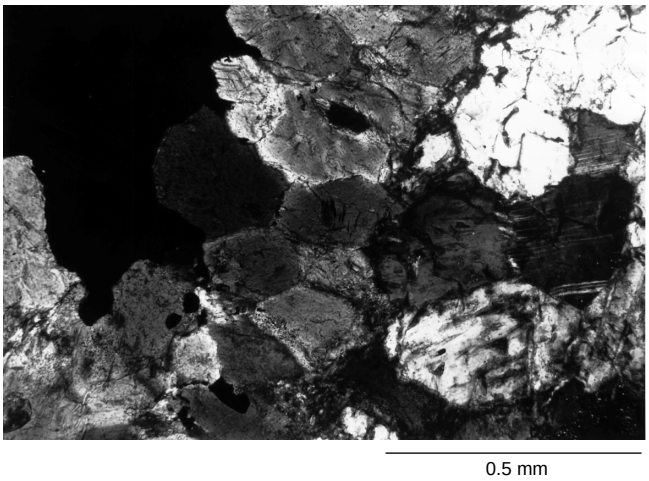

Figure 31. Photomicrograph showing polygonal grains of brown amphibole, possibly representing dynamic recrystallization. Large black grain is ilmenite. Gabbro pegmatite (Sample 173-1070A-R-2, 103–106 cm; crossed polars).

polygonal, brown amphibole grains may be products of dynamic recrystallization (Fig. 31). In addition to these rare high-temperature deformation features, the plagioclase crystals are later cut by microfractures from which sericitized zones extend. Brittle deformation also occurs in veins of calcite and vesuvianite. Sector and lamellar twinned 0.1- to 0.2-mm subhedral crystals of vesuvianite are fragmented in a matrix of microcrystalline calcite. Elsewhere, the gabbro is cut by veins that contain serpentine minerals.

The nature of the contact between the pegmatitic gabbro (Subunit 2A) and the serpentinized peridotite (Subunit 2B) is almost certainly

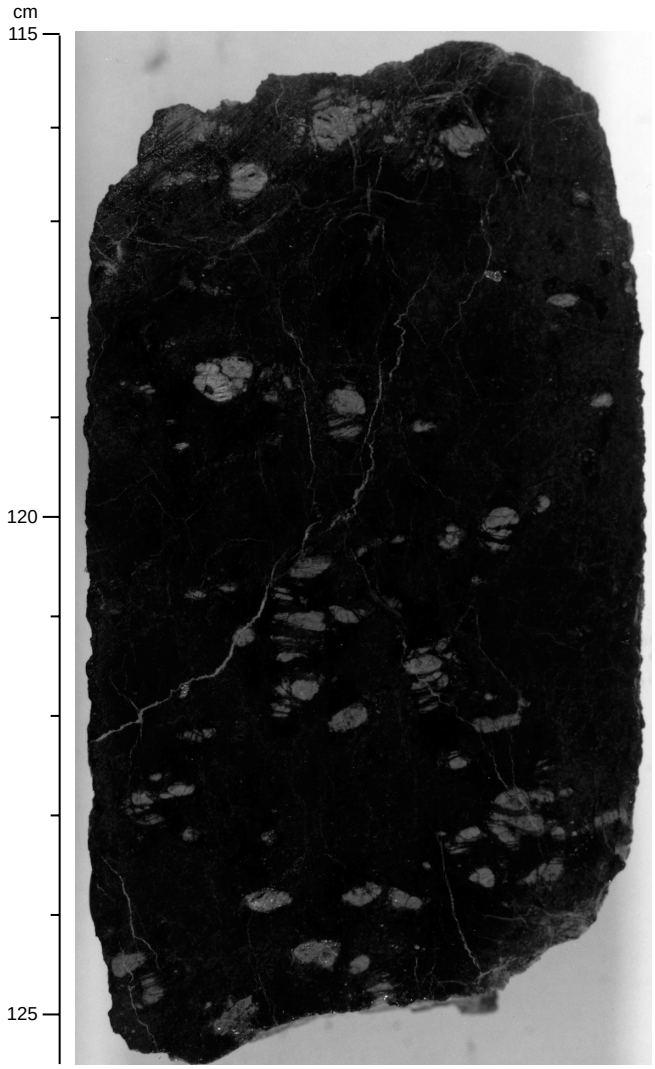

Figure 32. High-temperature foliation in serpentinized peridotite. Foliation is defined by alignment of pale pseudomorphed pyroxene (interval 173-1070A-10R-1, 115–125.5 cm).

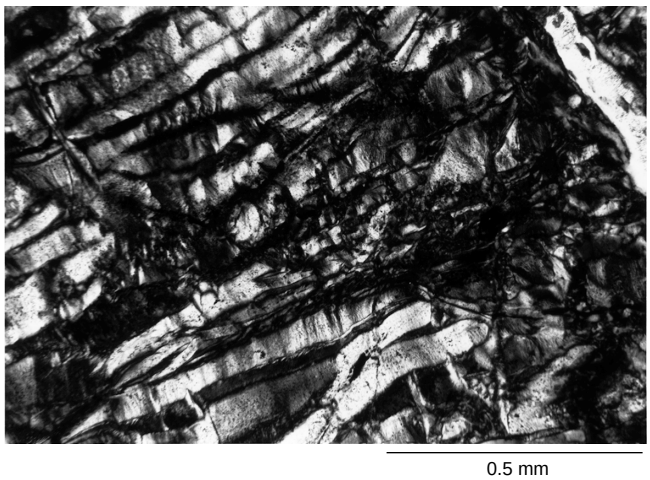

Figure 33. Photomicrograph showing foliation(?) in serpentinized peridotite formed by preferential alignment of small serpentine veins (Sample 173-1070A-14R-1, 31–36 cm; crossed polars).

intrusive. In interval 1070A-9R-3, 67–76 cm, gabbro pegmatite is juxtaposed against serpentinized dunite.

Subunit 2B: Serpentinized Peridotite

Serpentinization is pervasive throughout Subunit 2B. However, the least serpentinized peridotite is preserved toward the base of the core. In parts of Cores 1070A-13R and 14R, small olivine grains are preserved within the serpentine mesh structure (see "Igneous and Metamorphic Petrology" section, this chapter).

The serpentinized peridotite was locally weakly foliated at high temperature, prior to serpentinization. The high-temperature foliation occurs only sporadically throughout the core. It is defined by the preferred alignment of pseudomorphs after pyroxene (Fig. 32) and spinels. Remarkably, the coarse-grained spinel does not exhibit any preferred orientation. Where distinct, this foliation is moderately inclined (9° to 45°). In some samples, a low-temperature foliation is formed by preferential alignment of small, but abundant, serpentine veins (e.g., Sample 173-1070A-14R-1, 31–36 cm; Fig. 33). This texture can be described as a strongly elongated mesh texture.

Subunit 2B is cut by several (five in 30 m) gabbroic melt conduits or magmatic veins (see "Igneous and Metamorphic Petrology" section, this chapter). They are moderately to steeply inclined (two measurements: 51° and 62°). Traces of high-temperature deformation within the serpentinized peridotite appear to indicate a more intense deformation in the vicinity of one of the magmatic veins. These magmatic veins have formed preferred pathways for late-stage serpentine veins and associated complex hydrothermal alteration. Elsewhere, serpentine veins show no preferred orientation. Some pale green to white, 1- to 3-mm-thick veins contain deformed relicts of earlier, dark green, <1-mm-thick veins (similar to observations made in Hole 1068A, see "Structural Geology" section, "Site 1068" chapter, this volume).

Discussion

The basement/sediment contact encountered in Hole 1070A is similar to that in Hole 1068A, in that a basement of strongly serpentinized but nonmylonitic peridotite is overlain by a tectonosedimentary breccia along a fault contact marked by poorly lithified serpentinite gouge. In both holes, the lower part of the breccia appears to be of tectonic origin and the upper part of sedimentary origin. However, the clearly sedimentary part is much thinner in Hole 1070A than in Hole 1068A, and the clast spectrum is different (serpentinite and minor gabbro/anorthosite in Hole 1070A, metagabbro, meta-anorthosite, meta-tonalite, and amphibolite in Hole 1068A). Because a comparable breccia was also found during Leg 149 (Site 897), it appears that exhumed mantle in the Iberia Abyssal Plain is typically overlain by tectonosedimentary breccia, suggesting that the breccia may result from exhumation of the mantle along brittle normal faults and exposure of the shattered fault rocks at the seafloor. The absence of significant mylonitic deformation in the mantle rocks at Holes 1070A and 1068A and the occurrence of ultramylonitic shear bands only locally at Site 897 contrast with the intense ductile deformation observed in the Site 900 metagabbro and in the upper amphibolites of Site 1067.

Table 7. Carbonate, carbon, and nitrogen in sediments from Hole 1070A.

Core, section, interval (cm)	Depth (mbsf)	Inorganic C (wt%)	$CaCO_3$ (wt%)	Organic C (wt%)	N (wt%)	Organic C/N
173-1070A-						
1R-1, 22-23	599.22	0.21	1.7	0.13	0.07	1.9
1R-1, 26-29	599.26	2.03	16.9	0.00	0.08	
2R-1, 133-134	610.03	0.05	0.4	0.00	0.07	
2R-4, 18-19	613.38	0.12	1.0	0.00	0.06	
3R-1, 104-105	619.34	0.32	2.7	0.00	0.12	
4R-2, 46-48	629.86	0.30	2.5	0.00		
4R-4, 12-14	632.02	0.20	1.7	0.18	0.07	2.6
5R-1, 56-58	638.16	0.13	1.1	0.00	0.08	
5R-3, 39-41	640.49	0.07	0.6	0.22		
6R-1, 64-66	647.84	0.05	0.4	0.00	0.04	
6R-2, 97-99	649.67	0.05	0.4	0.12		
6R-3, 90-92	651.10	0.06	0.5	0.00		
7R-1, 26-28	657.16	0.09	0.7	0.00	0.04	

ORGANIC AND INORGANIC GEOCHEMISTRY

Concentrations of carbonate, organic carbon, and total nitrogen in sediments from Hole 1070A were measured on one to three samples per core. Routine measurements were also made of headspace gas compositions as part of the drilling safety program. Two interstitial water samples were squeezed from the sediments at 600.40 and 630.75 mbsf. Sediments from below the latter depth were too lithified to make interstitial water sampling possible.

Inorganic and Organic Carbon

Concentrations of carbonate carbon in sediments at Site 1070 are very low (0.05% to 2.03%), equivalent to $CaCO_3$ concentrations (assuming that all the carbonate is present as pure calcite) of 0.4% to 17% (Table 7). Concentrations of organic carbon are also low (0 to 0.22%).

Headspace Gas Measurements

Methane concentrations in headspace gases from sediments in Hole 1070A were very low (Table 8), consistent with the very low organic carbon contents of the sediments.

Interstitial Water

The compositions of two interstitial water samples collected from Hole 1070A are reported in Table 9.

PHYSICAL PROPERTIES

At Site 1070, magnetic susceptibility and natural gamma radiation were measured on all sedimentary cores and on intact basement sections longer than 20 cm. The sampling interval was 3 cm for magnetic susceptibility and 10 cm for natural gamma radiation measurements. All measurements of acoustic velocity used the Hamilton Frame Ve-

Table 8. Methane concentrations in headspace gas samples from Hole 1070A.

Core, section, interval (cm)	Depth (mbsf)	Methane (ppm)
173-1070A-		
1R-1, 149-150	600.49	3
2R-3, 145-150	613.15	3
3R-2, 0-5	619.80	3
4R-2, 133-135	630.73	3
5R-3, 64-65	640.74	3
6R-2, 149-150	650.19	3
7R-1, 85-90	657.75	3

Note: No heavier hydrocarbons were found in any of the gas samples.

Table 9. Interstitial water chemistry data for Hole 1070A.

Core, section, interval (cm)	Depth (mbsf)	SO_4^{2-} (mM)	K^+ (mM)	Cl^- (mM)	Ca^{2+} (mM)	Mg^{2+} (mM)	Na^+ (mM)
173-1070A-							
1R-1, 140-150	600.40	13.3	3.2	531	30.0	31.8	432
4R-2, 135-150	630.75	12.1	3.1	550	33.5	27.0	456

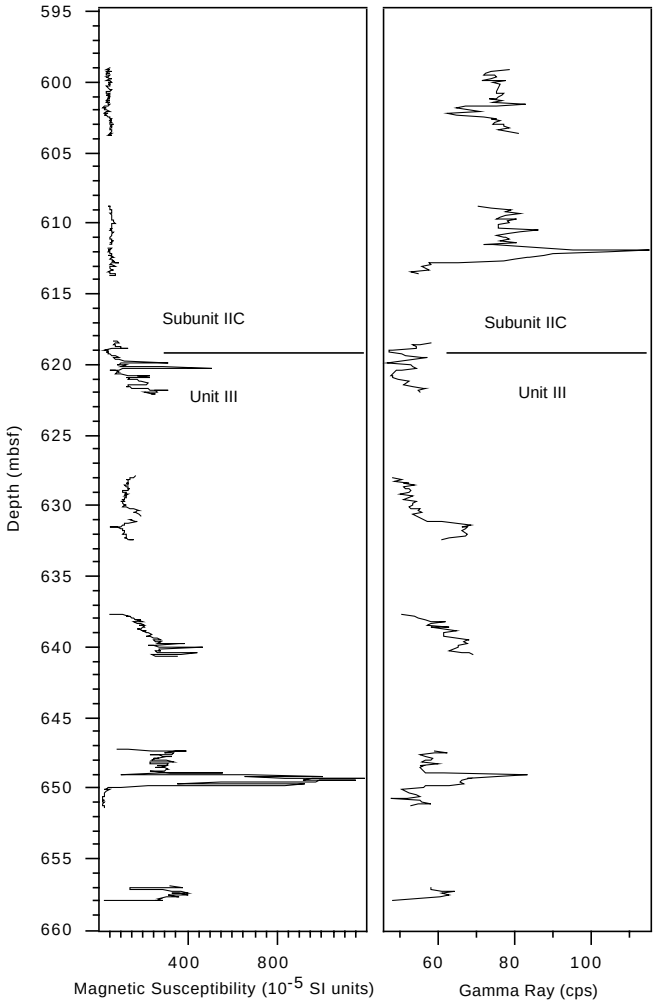

Figure 34. Magnetic susceptibility and natural gamma-ray activity vs. depth for the sedimentary section at Hole 1070A.

locimeter. Index properties of all samples from Hole 1070A included bulk density, grain density, porosity, water content, and void ratio.

Multisensor Track

The magnetic susceptibility and natural gamma radiation of sediment and basement cores from Hole 1070A are displayed in Figures 34 and 35, respectively. Values are listed in Tables 10 and 11 on CD-ROM (back pocket, this volume). In the sediments, magnetic susceptibility is generally low in Subunit IIC, varying from 40 to 80×10^{-5} SI units. Natural gamma-ray activity is between 70 and 80 cps. Both gamma-ray and magnetic susceptibility profiles exhibit a local minimum around 602 mbsf (Sample 173-1070A-1R-3, 5 cm), while the gamma-ray profile has a peak at 612 mbsf (Sample 173-1070A-2R-3, 25 cm) of 115 cps that is uncorrelatable with any feature in the magnetic susceptibility trace. Magnetic susceptibility in Unit III increases substantially, to between 100 and 400×10^{-5} SI units, while natural gamma-ray activity decreases to between 60 and 70 cps. Both magnetic susceptibility and gamma-ray activity exhibit a maximum at 649 mbsf (Sample 173-1070A-6R-2, 71 cm: sandy clay constituents), and there is a general correlation between the trends of the two properties throughout the unit.

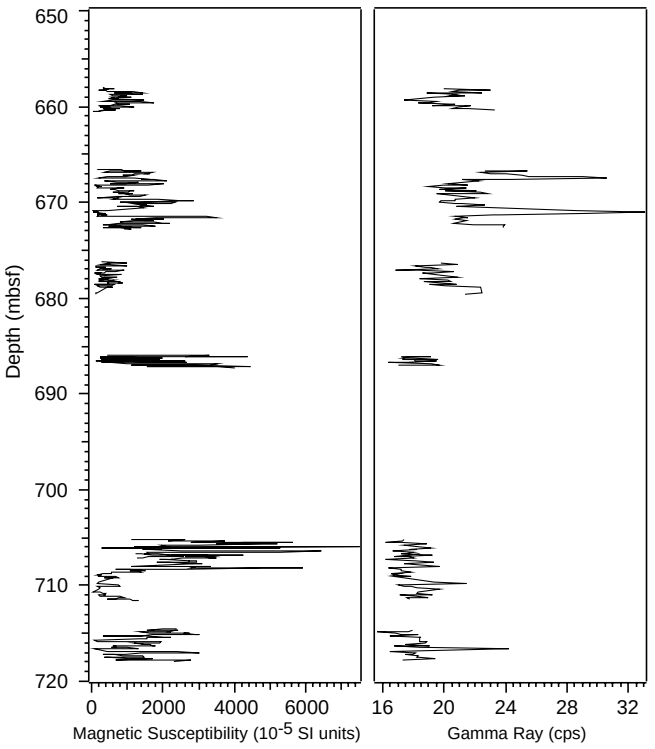

Figure 35. Magnetic susceptibility and natural gamma-ray activity vs. depth for the basement section at Hole 1070A.

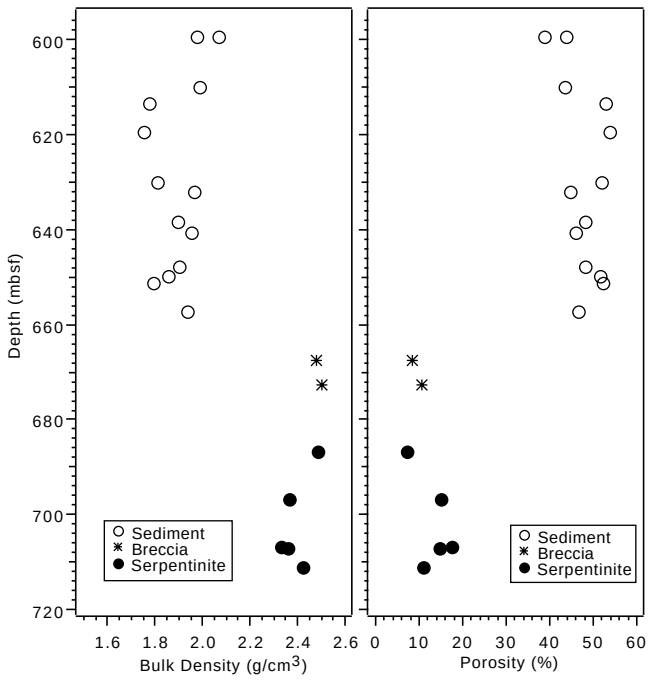

Figure 36. Bulk density and porosity of discrete samples vs. depth at Hole 1070A.

Table 12. Index properties of samples from Hole 1070A.

Core, section, interval (cm)	Depth (mbsf)	Bulk density (g/cm^3)	Grain density (g/cm^3)	Porosity (%)	Water content (% wet mass)	Lithology
170-1070A-						
1R-1, 20-22	599.2	1.98	2.72	44	29	Clay
1R-1, 27-29	599.27	2.07	2.73	39	24	Chalk
2R-1, 133-135	610.03	1.99	2.72	43	29	Clay
2R-4, 19-21	613.39	1.78	2.62	53	44	Clay
3R-1, 102-104	619.32	1.75	2.60	54	46	Clay
4R-2, 46-48	629.86	1.81	2.66	52	42	Clay
4R-4, 12-14	632.02	1.96	2.72	45	30	Clay
5R-1, 56-58	638.16	1.90	2.71	48	35	Clay
5R-3, 39-41	640.49	1.95	2.74	46	32	Clay
6R-1, 64-66	647.84	1.90	2.72	48	35	Clay
6R-2, 97-99	649.67	1.86	2.74	52	40	Sandy clay
6R-3, 90-92	651.1	1.79	2.63	52	43	Clay
7R-1, 26-28	657.16	1.93	2.73	47	33	Clay
8R-1, 117-119	667.67	2.48	2.61	9	4	Breccia
8R-5, 52-54	672.57	2.50	2.68	11	5	Breccia
10R-1, 95-97	686.85	2.49	2.60	7	3	Serpentinized peridotite
11R-2, 29-31	696.89	2.37	2.60	15	7	Serpentinized peridotite
12R-2, 83-85	706.79	2.33	2.61	17	8	Serpentinized peridotite
13R-1, 50-52	707.1	2.36	2.59	15	7	Serpentinized peridotite
13R-4, 68-70	711.25	2.42	2.60	11	5	Serpentinized peridotite

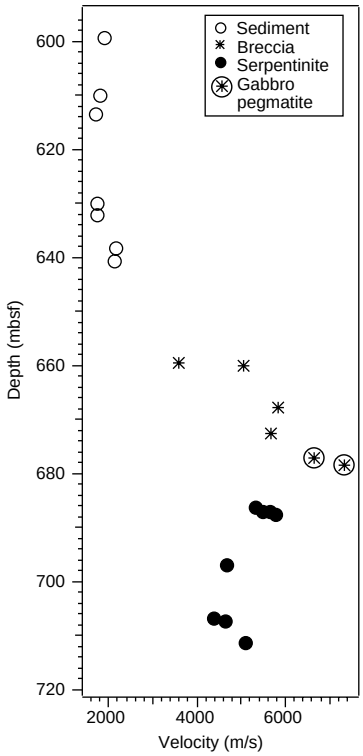

Figure 37. Compressional-wave velocity vs. depth at Hole 1070A.

In general, basement rocks have much higher values of magnetic susceptibility and lower values of natural gamma radiation than the overlying sediments. Magnetic susceptibility varies from a few hundred $\times 10^{-5}$ SI units to over 4000×10^{-5} SI units in the breccia, which comprises mainly clasts of serpentinized peridotite. The highest values are seen in the massive serpentinized peridotite below 685 mbsf (Fig. 35). Natural gamma radiation is around 20 cps in the breccias and drops to less than 20 cps in the serpentinized peridotite, except at 717 mbsf.

Table 13. Compressional-wave velocity data from Hole 1070A.

Core, section, interval (cm)	Depth (mbsf)	Velocity (m/s)	Lithology
173-1070A-			
1R-1, 27	599.27	1880	Brown clay
2R-1, 133	610.03	1786	Light green chalk
2R-4, 19	613.39	1698	Brown clay
4R-2, 46	629.86	1731	Brown clay
4R-4, 12	632.02	1734	Brown clay
5R-1, 56	638.16	2164	Brown clay
5R-3, 39	640.49	2123	Brown clay
7R-3, 30	659.53	3597	Serpentinite clast
7R-3, 80	660.03	5044	Fine-grained breccia
8R-1, 117	667.67	5842	Serpentinite clast
8R-5, 52	672.57	5663	Breccia
9R-1, 95	677.15	6645	Coarse gabbro
9R-2, 67	678.35	7342	Coarse gabbro
10R-1, 15	686.05	5302	Serpentinized peridotite
10R-1, 95	686.85	5555	Serpentinized peridotite
10R-2, 28	687.60	5775	Pyroxenite
11R-2, 29	696.89	4672	Serpentinized peridotite
12R-2, 83	706.79	4376	Serpentinized peridotite
13R-1, 50	707.10	4620	Serpentinized peridotite
13R-4, 68	711.25	5087	Serpentinized peridotite

Index Properties

Bulk densities and porosities of discrete samples of both basement and sediments are displayed vs. depth in Figure 36 and are listed in Table 12. Sediments at Site 1070 consist almost entirely of poorly consolidated clays. Bulk densities are generally between 1.8 and 2.0 g/cm^3, with the single chalk sample having a bulk density of 2.07 g/cm^3 (599 mbsf). Porosity is correspondingly high, with all samples except the chalk having porosities greater than 40%. Basement rocks have much higher bulk densities. The densities of the two breccia samples are ~2.7 g/cm^3, while the serpentinized peridotite samples vary between 2.5 and 2.3 g/cm^3. Porosity ranges from 7% to 17% in the basement rocks. Grain densities in both sediment and basement samples average around 2.65 g/cm^3, while serpentinized peridotites deviate only slightly from 2.6 g/cm^3.

Acoustic Velocities

Compressional-wave velocity at Site 1070 is plotted vs. depth in Figure 37 and tabulated in Table 13. The unconsolidated clay sedi-

ments are the slowest of any measured during Leg 173, with only two samples, located near the contact with basement, exceeding 2000 m/s. Basement rock velocities are much faster with all but one exceeding 4000 m/s; two gabbro pegmatite samples have velocities greater than 6000 m/s. These samples contained large (>3 cm) amphibole crystals; consequently, the high velocities are representative of amphibole crystals alone and not of the gabbro as a whole.

SUMMARY AND CONCLUSIONS

Summary

The history of this site began with the evolution of the mantle rocks leading up to their exposure on the seafloor, including the formation of the intrusive pegmatitic gabbro and of the tectonic breccia that caps the massive serpentinized peridotites. The preliminary shipboard studies give only some of the main characteristics of these rocks, which allow us to make a succinct comparison with the peridotites recovered further east at Sites 897 and 1068.

The original composition and texture of the peridotites are hardly recognizable because of the strong serpentinization of the rocks (up to 95%). Original spinels and relatively abundant relicts of clinopyroxene and smaller relicts of olivine are preserved. Rare chlorite patches, locally rimming spinels, may be derived from former plagioclase. These observations indicate that the mantle rocks were spinel-bearing and, at least locally, plagioclase-bearing peridotites. The serpentinized peridotite displays variable amounts of pyroxene, from pyroxenitic layers to more dunitic ones, pointing to a high degree of heterogeneity of the mantle. Protolithic assemblages suggest that the peridotites were lherzolites, harzburgites, and dunites, grading locally into pyroxenites. The size of the relict crystals of spinel, olivine, and some pyroxene suggests the former peridotites had a medium- to coarse-grained texture. In some samples, olivine exhibits kink bands, but pyroxenes are mostly undeformed with irregular shapes. A high-temperature foliation is only locally and weakly defined by the alignment of pseudomorphed pyroxenes. Remarkably, the coarse-grained spinel does not exhibit any preferred orientation. This apparent absence of high-temperature deformation suggests that the mantle rocks did not undergo intense deformation during their exhumation. The preliminary shipboard geochemical analyses indicate that these peridotites are compositionally close to the less plagioclase-rich peridotites of Site 897 (Leg 149) and Site 1068, provided that the actual geochemical signature is representative of initial rock composition. In addition to the small proportion of plagioclase, Site 1070 peridotites differ from those of the other two sites by having a smaller proportion of coarser grained spinel, a larger grain size, and a poorly developed or absent high-temperature deformation.

The peridotites contain small intrusive bodies and veins of coarse-grained altered gabbro, which could be related to the overlying pegmatitic gabbro. The presence of these intrusives suggests that the magmatic intrusions might have occurred relatively late during the evolution of the mantle when it already had a brittle behavior. An intrusive contact separates the serpentinized peridotites from the overlying 2.50-m-thick layer of pegmatitic gabbro. Although no shipboard geochemical analyses are available for these very coarse-grained rocks, their original igneous mineralogy, which is locally well preserved (plagioclase, red-brown amphibole, pyroxene, ilmenite, red biotite), suggests that they are differentiated products from melts derived from partial melting of the upper mantle. The gabbro is generally isotropic, except in local shear zones where there is limited dynamic recrystallization of plagioclase and amphibole. The rocks were then altered (low-grade overprint) under static conditions, down to very low-grade conditions under which the rocks were fractured and veined.

A thin interval of highly sheared serpentinite microbreccia marks the transition to the overlying tectonic breccia, which constitutes the top of the acoustic basement. This breccia is of matrix-supported serpentinized peridotite type, the matrix of which is formed by several generations of calcite. A tectonic origin is suggested by abundant "jigsaw" clasts and the transition downward into an incohesive fault gouge. The clasts mostly consist of serpentinized peridotite with characteristics comparable to those cored in the deeper part of the section and a few clasts consist of metagabbro.

The first sediments were deposited in the upper Aptian, probably at bathyal depths. They consist of matrix-supported sedimentary breccias, interbedded with a thin nannofossil pelagic chalk. The breccias are likely small debris flows or turbidites. There is a sharp contact with the overlying 39 m of barren brown claystone. The claystone is probably the result of slow accumulation of clay in a oxygenated environment on the abyssal plain below the CCD. It contains a thin horizon of umber and volcaniclastic sediments, small amounts of hematite, and a large proportion of botryoidal manganese nodules. The uppermost 20 m of the cored section was deposited in late Eocene to early Oligocene time. It consists of upward-darkening sequences of calcareous to nannofossil claystone overlain by claystone that were deposited as calcareous turbidites and noncarbonate hemipelagites, probably below the CCD.

Conclusion

No rocks of the upper oceanic crust were found at Site 1070, which was expected to be located on the first accreted oceanic crust. The presence of mantle rocks and associated products of partial melting indicates that the zone of mantle exposure in the transition zone between the continental crust and the true oceanic crust is wider than previously supposed. An interesting fact is that the mantle along the west edge of the OCT is not similar to that cored further east at Sites 897 and 1068. The main differences are the lower initial plagioclase mode, the coarser grain size, and the near-lack of high-temperature foliation for Site 1070 partially serpentinized peridotites. Further studies are needed to better constrain the nature and evolution of the mantle rocks and of the associated subordinate pegmatitic gabbros cored at Site 1070, and to establish the relationships between these mafic and ultramafic rocks and the chronology of intrusion. These studies on the evolution of the mantle along the west edge of the OCT will tentatively help to determine the geodynamic evolution from continental rifting to seafloor spreading.

REFERENCES

Beslier, M.O., Ask, M., and Boillot, G., 1993. Ocean-continent boundary in the Iberia abyssal plain from multichannel seismic data. *Tectonophysics*, 218:383–393.

Boillot, G., Agrinier, P., Beslier, M.-O., Cornen, G., Froitzheim, N., Gardien, V., Girardeau, J., Gil-Ibarguchi, J.-I., Kornprobst, J., Moullade, M., Schaerer, U., and Vanney, J.-R., 1995. A lithospheric syn-rift shear zone at the ocean-continent transition: preliminary results of the GALINAUTE II cruise (Nautile dives on the Galicia Bank, Spain). *C. R. Acad. Sci. Ser 2a*, 321:1171–1178.

Boillot, G., Comas, M.C., Girardeau, J., Kornprobst, J., Loreau, J.-P., Malod, J., Mougenot, D., and Moullade, M., 1988. Preliminary results of the Galinaute cruise: dives of the submersible *Nautile* on the Western Galicia Margin, Spain. *In* Boillot, G., Winterer, E.L., et al., *Proc. ODP, Sci. Results*, 103: College Station, TX (Ocean Drilling Program), 37–51.

Boillot, G., Grimaud, S., Mauffret, A., Mougenot, D., Kornprobst, J., Mergoil-Daniel, J., and Torrent, G., 1980. Ocean-continent boundary off the

Iberian margin: a serpentinite diapir west of the Galicia Bank. *Earth Planet. Sci. Lett.*, 48:23–34.
Bown, J.W., and White, R.S., 1995. Finite duration rifting, melting and subsidence at continental margins. *In* Banda, E., Torne, M., and Talwani, M. (Eds.), *Rifted Ocean/Continent Boundaries.* NATO ASI Ser. C: Math. Phys. Sci., 463:31–54.
Cannat, M., 1993. Emplacement of mantle rocks in the seafloor at mid-ocean ridges. *J. Geophys. Res.*, 98:4163–4172.
Cannat, M., Karson, J.A., Miller, D.J., et al., 1995. *Proc. ODP, Init. Repts.*, 153: College Station, TX (Ocean Drilling Program).
Cornen, G., Beslier M.-O., and Girardeau, J., 1996. Petrologic characteristics of the ultramafic rocks from the ocean/continent transition in the Iberia Abyssal Plain. *In* Whitmarsh, R.B., Sawyer, D.S., Klaus, A., and Masson, D.G. (Eds.), *Proc. ODP, Sci. Results*, 149: College Station, TX (Ocean Drilling Program), 377–395.
Dean, S.M., Minshull, T.A., Whitmarsh, R.B., Louden, K., and Chian, D., 1996. A seismic study of the ocean-continent transition in the Iberia Abyssal Plain. *Eos*, 77:F668.
Girardeau, J., Cornen, G., Agrinier, P., Beslier, M.O., Dubuisson, G., Le Gall, B., Monnier, C., Pinheiro, L., Ribeiro, A., and Whitechurch, H., in press. Résultats des plongées du *Nautile* sur le Banc de Gorringe. *C.R. Acad. Sci. Ser. 2.*
Kornprobst, J., Vidal, P., and Malod, J., 1988. Les basaltes de la Marge de Galice (NO de la Péninsule Ibérique): hétérogénéité des spectres de terres rares à la transition continent/océan. Données géochimiques préliminaires. *C. R. Acad. Sci. Ser. 2*, 306:1359–1364.
Malod, J.A., Murillas, J., Kornprobst, J., and Boillot, G., 1993. Oceanic lithosphere at the edge of a Cenozoic active continental margin (northwestern slope of Galicia Bank, Spain). *Tectonophysics*, 221:195–206.
Martini, E., 1971. Standard Tertiary and Quaternary calcareous nannoplankton zonation. *In* Farinacci, A. (Ed.), *Proc. 2nd Int. Conf. Planktonic Microfossils Roma:* Rome (Ed. Tecnosci.), 2:739–785.
Masson, D.G., and Miles, P.R., 1984. Mesozoic seafloor spreading between Iberia, Europe and North America. *Mar. Geol.*, 56:279–287.
Matthews, D.H., 1962. Altered lavas from the floor of the eastern North Atlantic. *Nature*, 194:368–369.
Rabinowitz, P.D., Cande, S.C., and Hayes, D.E., 1978. Grand Banks and J-Anomaly Ridge. *Science*, 202:71–73.
————, 1979. The *J*-anomaly in the central North Atlantic Ocean. *In* Tucholke, B.E., and Vogt, P.R., et al., *Init. Repts. DSDP*, 43: Washington (U.S. Govt. Printing Office), 879–885.
Sawyer, D.S., Whitmarsh, R.B., Klaus, A., et al., 1994. *Proc. ODP, Init. Repts.*, 149: College Station, TX (Ocean Drilling Program).
Seifert, K., and Brunotte, D., 1996. Geochemistry of serpentinized mantle peridotite from Site 897 in the Iberia Abyssal Plain. *In* Whitmarsh, R.B., Sawyer, D.S., Klaus, A., and Masson, D.G. (Eds.), *Proc. ODP, Sci. Results*, 149: College Station, TX (Ocean Drilling Program), 413–424.
Shipboard Scientific Party, 1994a. Site 897. *In* Sawyer, D.S., Whitmarsh, R.B., Klaus, A., et al., *Proc. ODP, Init. Repts.*, 149: College Station, TX (Ocean Drilling Program), 41–113.
————, 1994b. Site 899. *In* Sawyer, D.S., Whitmarsh, R.B., Klaus, A., et al., *Proc. ODP, Init. Repts.*, 149: College Station, TX (Ocean Drilling Program), 147–209.
————, 1994c. Site 900. *In* Sawyer, D.S., Whitmarsh, R.B., Klaus, A., et al., *Proc. ODP, Init. Repts.*, 149: College Station, TX (Ocean Drilling Program), 211–262.
————, 1994d. Site 901. *In* Sawyer, D.S., Whitmarsh, R.B., Klaus, A., et al., *Proc. ODP, Init. Repts.*, 149: College Station, TX (Ocean Drilling Program), 263–268.
Sibuet, J.-C., Louvel, V., Whitmarsh, R.B., White, R.S., Horsefield, S.J., Sichler, B., Leon, P., and Recq, M., 1995. Constraints on rifting processes from refraction and deep-tow magnetic data: the example of the Galicia continental margin (West Iberia). *In* Banda, E., Torné, M., and Talwani, M. (Eds.), *Rifted Ocean-Continent Boundaries:* Amsterdam (Kluwer), 197–218.
Tucholke, B.E., and Ludwig, W.J., 1982. Structure and origin of the J anomaly Ridge, western North Atlantic Ocean. *J. Geophys. Res.*, 87:9389–9407.
White, R.S., and McKenzie, D., 1989. Magmatism at rift zones: the generation of volcanic continental margins and flood basalts. *J. Geophys. Res.*, 94:7685–7729.
White, R.S., McKenzie, D., and O'Nions, R.K., 1992. Oceanic crustal thickness from seismic measurements and rare earth element inversions. *J. Geophys. Res.*, 97:19683–19715.
Whitmarsh, R.B., and Miles, P.R., 1994. Propagating rift model for the West Iberia rifted margin based on magnetic anomalies and ODP drilling. *Eos*, 75:616.
————, 1995. Models of the development of the West Iberia rifted continental margin at 40°30′N deduced from surface and deep-tow magnetic anomalies. *J. Geophys. Res.*, 100:3789–3806.
Whitmarsh, R.B., Miles, P.R., and Mauffret, A., 1990. The ocean-continent boundary off the western continental margin of Iberia, I. Crustal structure at 40°30´N. *Geophys. J. Int.*, 103:509–531.
Whitmarsh, R.B., Miles, P.R., Sibuet, J.-C., and Louvel, V., 1996a. Geological and geophysical implications of deep-tow magnetometer observations near Sites 897, 898, 899, 900, and 901 on the west Iberia continental margin. *In* Whitmarsh, R.B., Sawyer, D.S., Klaus, A., and Masson, D.G. (Eds.), *Proc. ODP, Sci. Results*, 149: College Station, TX (Ocean Drilling Program), 665–674.
Whitmarsh, R.B., Pinheiro, L.M., Miles, P.R., Recq, M., and Sibuet, J.C., 1993. Thin crust at the western Iberia ocean-continent transition and ophiolites. *Tectonics*, 12:1230–1239.
Whitmarsh, R.B., and Sawyer, D.S., 1996. The ocean/continent transition beneath the Iberia Abyssal Plain and continental-rifting to seafloor-spreading processes. *In* Whitmarsh, R.B., Sawyer, D.S., Klaus, A., and Masson, D.G. (Eds.), *Proc. ODP, Sci. Results*, 149: College Station, TX (Ocean Drilling Program), 713–733.
Whitmarsh, R.B., White, R.S., Horsefield, S.J., Sibuet, J.-C., Recq, M., and Louvel., V., 1996b. The ocean-continent boundary off the western continental margin of Iberia: crustal structure west of Galicia Bank. *J. Geophys. Res.*, 101:28291–28314.
Zhao, X., 1996. Magnetic signatures of peridotite rocks from Sites 897 and 899 and their implications. *In* Whitmarsh, R.B., Sawyer, D.S., Klaus, A., and Masson, D.G. (Eds.), *Proc. ODP, Sci. Results*, 149: College Station, TX (Ocean Drilling Program), 431–446.

Ms 173IR-108

NOTE: For all sites drilled, core-description forms ("barrel sheets") and core photographs can be found in Section 3, beginning on page 295. Forms containing smear-slide data, sedimentary thin-section descriptions, and igneous/metamorphic thin-section descriptions can be found on CD-ROM. See Table of Contents for material contained on CD-ROM.

Prior Chapter Contents Next Chapter